ESD-TR-78-208

LEVEL II

Semiannual Technical Summary

Distributed Sensor Networks

31 March 1978

Prepared for the Defense Advanced Research Projects Agency
under Electronic Systems Division Contract F19628-78-C-0002 by

Lincoln Laboratory
MASSACHUSETTS INSTITUTE OF TECHNOLOGY
LEXINGTON, MASSACHUSETTS

The work reported in this document was performed at Lincoln Laboratory, a center for research operated by Massachusetts Institute of Technology. This work was sponsored by the Defense Advanced Research Projects Agency under Air Force Contract F19628-78-C-0002 (ARPA Order 3345).

This technical report has been reviewed and is approved for publication.

FOR THE COMMANDER

Raymond L. Loiselle

Raymond L. Loiselle, Lt. Col., USAF
Chief, ESD Lincoln Laboratory Project Office

MASSACHUSETTS INSTITUTE OF TECHNOLOGY

LINCOLN LABORATORY

(6) DISTRIBUTED SENSOR NETWORKS.

(9) SEMIANNUAL TECHNICAL SUMMARY REPORT. 1 Oct 77-31 Mar 78

TO THE

DEFENSE ADVANCED RESEARCH PROJECTS AGENCY

(10) Richard T. Lacoss

1 OCTOBER 1977 – 31 MARCH 1978

ISSUED 31 AUGUST 1978

(11) 31 Mar 78

(12) 63p.

(15) F19628-78-C-0002, ARPA Order-3345

Approved for public release; distribution unlimited.

(18) ESD

(19) TR-78-208

LEXINGTON MASSACHUSETTS

ABSTRACT

Progress on the Distributed Sensor Networks program is reported. Topics covered in the sensor area are the performance of acoustic sensors, sizing of acoustic front-end computation requirements, feasibility of adapting packet radios to perform as radar sensors, and a preliminary investigation of IR options. In all cases, the targets considered were low-flying aircraft or cruise missiles. Progress is reported in the area of decision theoretic surveillance space search methods of multisite detection and on specific algorithms to locate targets using two acoustic sites. Results of a preliminary parametric sensor and system cost analysis are given.

CONTENTS

CONTRIBUTORS
TO
DISTRIBUTED SENSOR NETWORKS PROGRAM

GROUP 22

Lacoss, R. T.
Demko, P.
Landers, T. E.
Walton, R. L.

GROUP 41

Goblick, T. J.

DISTRIBUTED SENSOR NETWORKS

I. INTRODUCTION AND SUMMARY

This is the second Semiannual Technical Summary (SATS) report of the Lincoln Laboratory Distributed Sensor Networks (DSN) program which is aimed at identifying and demonstrating innovative applications of new developments in computer network theory and computer science to systems employing multiple sensors for target surveillance and tracking. Such systems are made up of sensors, data bases, and processors distributed throughout an area, interconnected by an appropriate communication system, and serving users who are also distributed and served by the same communication system. A major hypothesis to be demonstrated is that through suitable netting and distributed processing, the information from individual sensors of limited capacity and/or range can be combined to yield an effective survivable surveillance system at feasible cost. The program is oriented around the eventual development of a testbed system, and demonstrations in the context of such a testbed. The testbed problem selected is the detection and tracking of low-flying aircraft and cruise missiles. This is an important application problem since terrain masking and clutter pose major difficulties for classical systems based upon larger ground-based surveillance radars.

Progress and results obtained during this reporting period are summarized below and presented in greater detail in subsequent sections of this report.

A. SENSORS

Our accomplishments in four sensor-related areas may be summarized as follows.

(1) We completed further evaluation of the performance of acoustic sensors, particularly acoustic arrays. Acoustic azimuth measurements from digital processing were demonstrated over a complete 30-km aircraft track. This was done in the presence of coherent directional interfering noise. The ability to discriminate on the basis of direction and frequency content was thus also demonstrated. We also verified that transmission-path variations make it very difficult to directly obtain aircraft elevation-angle information except when the elevation angle is very large. Measurements of coherence between microphones displaced by 0.6 km indicated that long baseline coherent combining of raw acoustic data will probably not be useful.

(2) We formulated and sized a number of strawman algorithms for detection at a small acoustic array. In general, it appears that the front-end signal processing and detection load will be too large for a typical minicomputer, but that it is easily within the capability of a minicomputer coupled with a modest amount of special-purpose signal-processing hardware.

(3) We completed a study to determine the feasibility of adapting packet radio to provide radar-sensor information to the DSN. A large number of options were considered. In general, we concluded that packet radio

could serve as a useful sensor for low-flying aircraft or cruise missiles only after undergoing very major changes with respect to power levels, signal waveforms, and antenna directionality. Even then, success might be marginal due to the frequency band of operation. The recommended approach is to develop effective small radars whose outputs would be distributed as required by colocated packet radios and interpreted by the DSN as a whole.

(4) We investigated the possible use of IR sensors, and established from the literature and from analysis that targets of interest will produce detectable signals at ranges of several kilometers. However, a substantial sensor-development effort would be required to determine if an appropriate DSN IR sensor could be developed. Critical engineering factors are cost, complexity, and the ability to operate unattended for long periods of time.

B. MULTISITE DETECTION

Work continues on the general problem of multisite detection, and particularly upon the use of acoustic azimuth measurements.

Experimental software has been developed and tested to investigate the characteristics and performance of the decision theoretic surveillance space search approach to multisite detection and location. A number of space and time quantization issues have been identified for future study. Using this software, we can now examine the capability of an acoustic system to function with multiple targets, false alarms, and errors in measurements.

A companion effort to develop specific algorithms to locate targets given only the time history of azimuth observations from two acoustic sites has been successful. Regions of poor location capability have been identified, as has the effect of aircraft altitude. These results provide insight into the performance of an acoustic system. The method may be used as an alternative or supplement to surveillance space search – most likely it is a supplement. This algorithm is not intended to provide optimum locations or tracking. It makes no assumptions about the dynamics or trajectories of targets.

C. GENERAL SYSTEM ANALYSIS

We have completed an analytical study of sensor cost and performance trade-offs. Factors considered were cost, sensor options for improving signal-to-noise ratios (SNRs), signal-propagation losses, and sensor ranges. Within the context of the study and the models used, the optimum choice of sensor range was determined. In general, this study was intended to identify and clarify some of the issues; it considered only a small number of the relevant factors.

II. SENSORS

Work has continued in the area of sensor options for the low-flying-aircraft problem. Acoustic and radar options continue to be investigated. We also initiated an investigation of the feasibility of infrared sensors.

The DSN acoustic sensor option remains the most developed option at this time. Additional data from our Fort Huachuca, Arizona field experiment were digitized and analyzed to further demonstrate the basic capabilities of these sensors to detect, locate, and separate multiple targets. Strawman algorithms for coherent acoustic array data reduction have been sized to verify that the required computation is not excessive and to indicate the scale of hardware requirements for an acoustic node of a DSN.

Our work in the radar-sensor area has intentionally been closely coupled to the characteristics of packet radios. We initiated and have essentially completed a study to determine if packet radios could be modified or evolved into units which could furnish sensor as well as communication functions for a DSN. Such a study was clearly required before investigation was begun into other radar options that do not utilize packet radio. We generally conclude that it is not possible to evolve packet radio into a sensor without very major changes to the packet radio. However, our study clearly indicated that the design of a low-power small-scale DSN radar for low-flying aircraft can probably be developed. A separate, unconstrained study of DSN radar options is recommended.

The investigation of DSN IR sensors for low-flying aircraft was limited to establishing that targets do produce detectable signals at ranges of several kilometers. An in-depth sensor design effort would be required to determine if an IR sensor appropriate for DSN use can be developed. The critical issues are cost, complexity, and ability to operate unattended for long periods of time.

Results of these sensor investigations are summarized in the following sections.

A. ACOUSTIC-SENSOR PERFORMANCE

Initial results of the Fort Huachuca acoustic experiment were presented in our first SATS.[1] Visual analysis of strip-chart recordings established that acoustic sensors have sufficient detection ranges to be of considerable use in a DSN for low-flying-aircraft surveillance. Processing a limited amount of digital data indicated that useful acoustic azimuth measurements could be obtained for acoustic source-receiver distances out to at least several kilometers. Since that time, additional digital data covering complete 30-km test tracks have been obtained. New processing results using the new data as well as some of the previously available data are presented in this section.

In general, we have concerned ourselves with the performance of an acoustic-only or an acoustic-aided DSN for the surveillance of multiple low-flying targets in the presence of noise due to either natural or artificial sources. To a large extent, acoustic-sensor performance depends upon the ability of array processing to separate incoming acoustic waves according to their arrival azimuth and phase velocity and upon spectral analysis to differentiate and characterize the nature of the source producing the acoustic energy.

TABLE II-1

ARRAY PROCESSING RESULTS FOR THE COMPLETE A-7 TRACK

Acoustic Range (km)	Acoustic Phase Velocity (m/sec)	Acoustic Azimuth (deg)	Radar Azimuth (deg)
−16.0	321	270	264
−11.3	371	249	264
−6.8	318	270	264
−4.0	329	261	262
−0.7	429	239	240
0.7	371	111	120
1.4	364	104	107
2.0	331	96	102
2.6	329	99	99
3.2	323	96	98
3.9	359	96	96
4.5	359	96	95
5.2	341	97	95
5.8	341	97	94
6.4	361	90	93
7.1	361	90	91
7.5	342	90	91
8.7	342	90	91
9.9	350	90	91
11.1	328	90	91
12.3	417	90	91
13.2	375	90	90
14.4	382	80	90

1. *Small-Aperture-Array Performance*

Table II-1 shows digital-data-analysis results for a complete jet-aircraft track. The basic analysis tool was frequency-wavenumber processing. The microphone array consisted of 9 sensors in a 5-m aperture. The jet aircraft flew approximately 200 m off the ground over the entire path. The data were processed to obtain azimuth measurements at approximately 5-sec intervals. Each processed data segment consisted of 1 sec of signal which was analyzed with 1-Hz resolution at 10-Hz intervals over the band 80 to 130 Hz. From the table, it can be seen that the aircraft was successfully tracked from 16 km inbound to 14.4 km outbound. These ranges are not necessarily the limiting tracking ranges, but correspond to the earliest and latest data recorded in the field. Note that, even though the data were analyzed in approximately equal time intervals, the range bins are not equispaced. This results from the moving source effect discussed in our last SATS.[1] The acoustic range was derived from the recorded radar tracking data.

Figure II-A-1 plots the observed acoustic azimuth against the acoustic range calculated from the radar tracking information. The calculated acoustic azimuth of the aircraft is indicated by the solid line. While a minor amount of scattering is present, the overall performance of the processing is good. In fact, the acoustic azimuths fall within the precision of the radar data over the complete track. The largest azimuthal deviations occur on the extremes of the path. In these regions the signal is more than 40 dB down from its peak amplitudes near the closest point of approach (CPA). In this situation, we are probably suffering from the limitations of the analog recording method used to obtain the digital data. Nevertheless, azimuth measurements could be made, even though (as shown below) a strong interfering noise background, which is several decibels above the aircraft noise, is present.

Figure II-A-2 shows the signals recorded across the array at the time the acoustic wave from the jet at a 16-km distance inbound would arrive. Clearly, a large coherent signal is propagating across the array and good array processing results should be expected. Figure II-A-3 shows the spectra of these signals in the 80- to 130-Hz band. (Unfortunately, the system noise outside this band was significant for the signal levels of interest.) The narrowband peaks in the spectra indicate that the signal is dominated by a piston-type source rather than the broadband signal one would associate with a jet source. Each of the peak frequencies was investigated in the wavenumber domain and found to originate from a constant direction. The results at 100 Hz are shown in Fig. II-A-4, where the arrows indicate the direction to the A-7 and the direction to the generator used in the experiment. The sound in this interval is dominated by the generator noise. Since we expect the jet to have acoustic energy distributed over the entire range, the wavenumber spectrum at a point between the harmonic-generator noise peaks was calculated. Figure II-A-5 shows the result at 90 Hz, where the signal power is down by about 10 dB from the generator peaks. As expected, the A-7 is detected with some interference from the generator sound field. In the region up to -6 km and beyond 14 km, the dominant signal was generator noise. Fortunately, because of the spectral nature of the noise and the signal, successful processing at a SNR of at least -10 dB was obtained. In general, because source type has a great influence on signal spectra, these results should be regarded as typical and not unusual. Improved array design and higher quality data collection will result in even better processing gains.

In theory, the elevation angle of an aircraft should be indicated by the phase velocity of the acoustic wave crossing the array. The observed phase-velocity values for the above experiment

are given in Table II-1. Despite the fact that the array resolution in phase velocity is about a meter/second, the observations fluctuate several tens of meters/second with respect to their predicted values based upon radar tracking and known aircraft altitude. This scatter corresponds to a standard deviation in elevation angle of more than 10° over the entire track. Such a scatter, probably caused by the velocity microstructure of the atmosphere, is too large for precision elevation-tracking purposes. Useful elevation-angle information can only be obtained when the true elevation angle is large relative to the scatter.

2. Larger-Aperture-Array Options

One question we have not previously addressed is whether coherent combining of raw acoustic data (as opposed to combining single-site azimuth or frequency measurements) from sites separated by several kilometers is possible. To some extent this is still an open question, but we do have some results which indicate that it may not be possible or practical. Fortunately, the ability to do such long-range coherent combining is not crucial for the functioning of a DSN. Further research in this area might be done in parallel with other future experimental and testbed efforts.

Using jet-aircraft (A-7) and helicopter (UH-1) data, we looked at long-range coherence by computing the cross-correlation between central array elements and the GRD microphone offset from the array by 600 m (see Ref. 1 for a complete description of the experiment). The 600-m distance is not as large as one would like to answer the questions, but it was the largest which could be obtained during the experiments. Figure II-A-6 shows the cross-correlation of the GRA and GRC elements of the central array. These microphones are located only 0.5 m apart. The signal was from a UH-1 helicopter. As expected, the peak correlation is high (0.9) and the envelope of the cross-correlation function decays very slowly due to the narrowband nature of the sound. The cross-correlation between the GRA and GRD instruments is shown in Fig. II-A-7; these instruments are located 600 m apart. Time differences of arrival corresponding to wavefront group velocities equal to the speed of sound, c, and equal to 600 m/sec are indicated in the figure. While, as one would predict, the envelope of the function peaks in this time-lag region, the envelope drops too slowly to be certain which peak to select. The dominant energy in the signal is about 40 Hz so that the wavelength is about 10 m. The maximum correlation is 0.4. Thus, over approximately 60 wavelengths the signal peak coherence drops by more than a factor of 2. In a poorer signal-to-noise environment, the resolution would be even worse. We are led to the result then that, over several tens of wavelengths for narrowband signals, acoustic path characteristics degrade signals to the point where coherent signal processing would provide minimal signal information. Figures II-A-8 and -9 show the same computation for the A-7. Jet acoustic sources are broadband, and the improvement in resolution is obvious even though the overall peak coherence is smaller (0.3 as opposed to 0.4 for the UH-1) than for the narrowband source. These preliminary results indicate that coherence of both broadband and narrowband sources will drop at sensor separations of a kilometer or more to the point that coherent processing of raw data will not be possible at all. On a preliminary basis, we conclude that the systematic combination of multiple small arrays will not be improved with long-range coherence of the actual acoustic signals. Fortunately, it should be possible to design and demonstrate an acoustic DSN without requiring such long baseline coherent processing. Further investigations of long baseline coherent processing could be a parallel longer-term research activity. Coherent processing of spectra (as opposed to time series) from widely separated sites is another area which could be studied in the future.

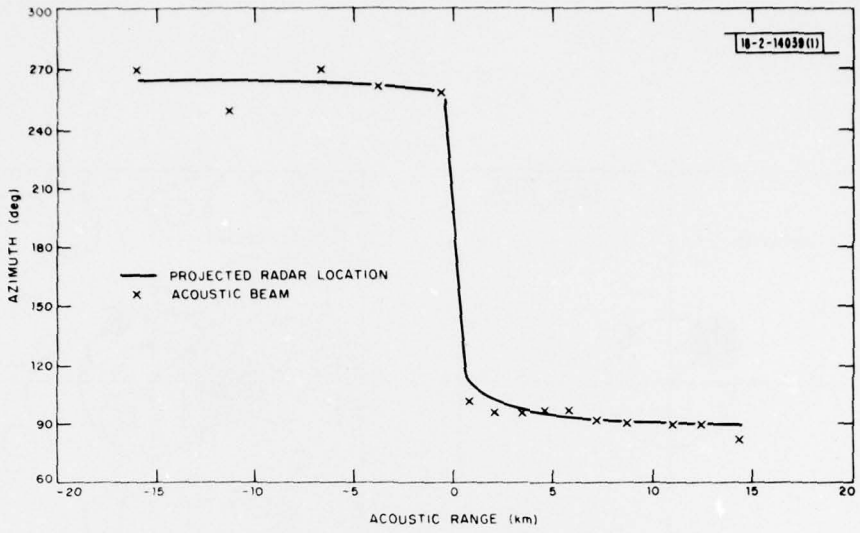

Fig. II-A-1. Azimuth detections over the complete A-7 track. 200 m altitude. Negative ranges are inbound.

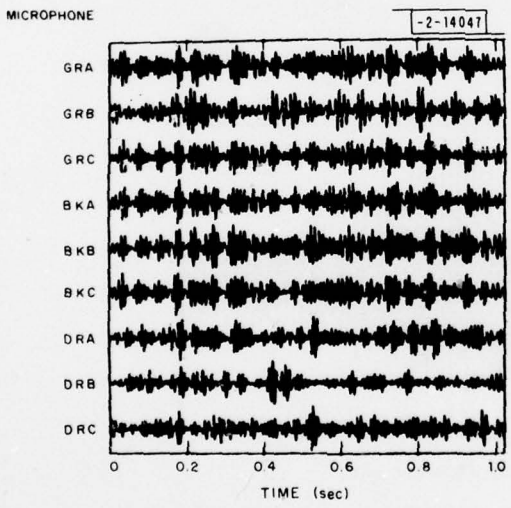

Fig. II-A-2. Acoustic signal recorded when A-7 was 16 km inbound. Note high signal coherence level across array. This narrowband coherent signal is noise from a nearby generator. The A-7 signal is not visible.

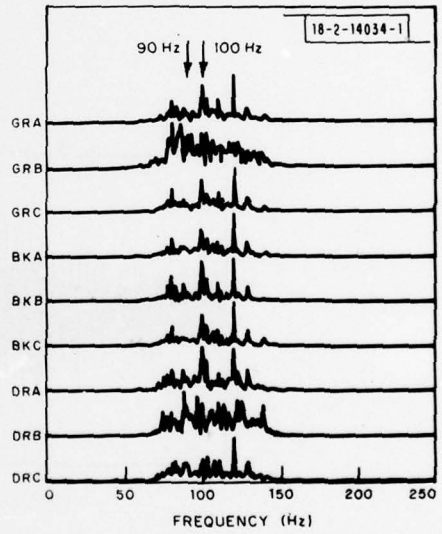

Fig. II-A-3. Spectra on a linear scale of signals shown in Fig. II-A-2. Narrowband peaks indicate signals are dominated by piston-type source rather than jet source. Peaks are about 10 dB above background.

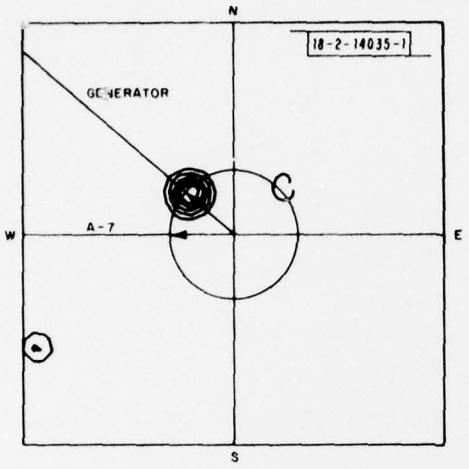

Fig. II-A-4. Wavenumber spectrum at 100 Hz. Arrows show generator and A-7 acoustic directions, respectively.

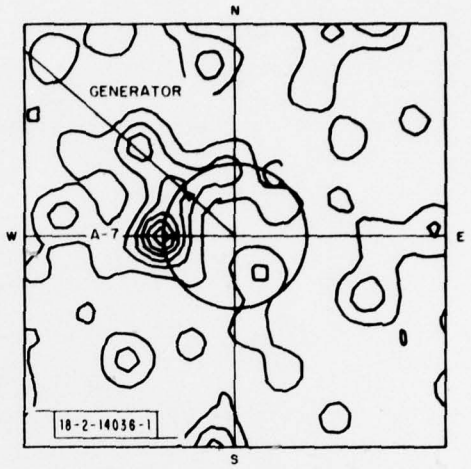

Fig. II-A-5. Wavenumber spectrum at 90 Hz indicates A-7 signal detection for a −10-dB SNR.

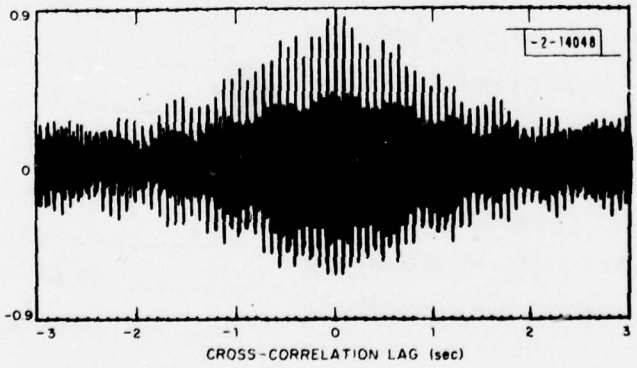

Fig. II-A-6. Cross-correlation of GRA-GRC for UH-1 signal. Station separation of 0.5 m.

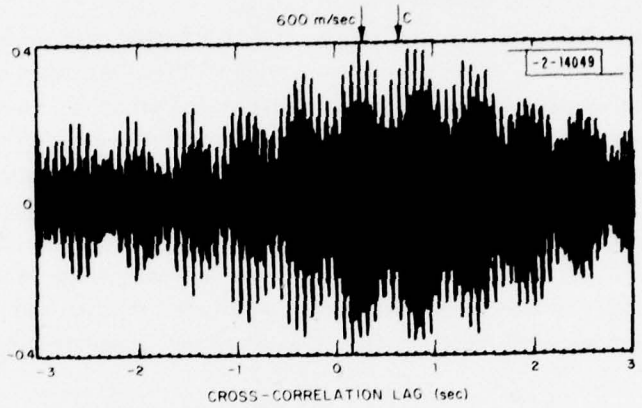

Fig. II-A-7. Cross-correlation of GRA-GRD for UH-1 signal. Station separation of 600 m.

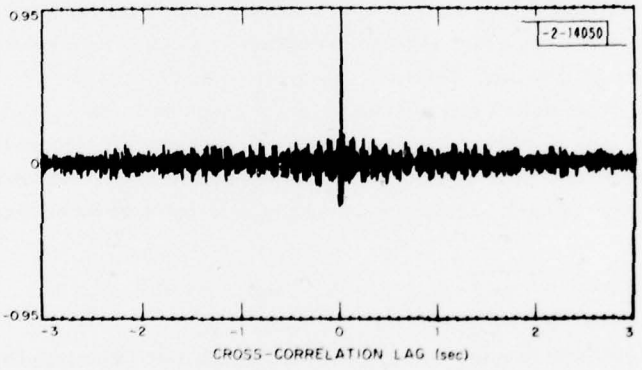

Fig. II-A-8. Cross-correlation of GRA-GRC for A-7 signal. Station separation of 0.5 m.

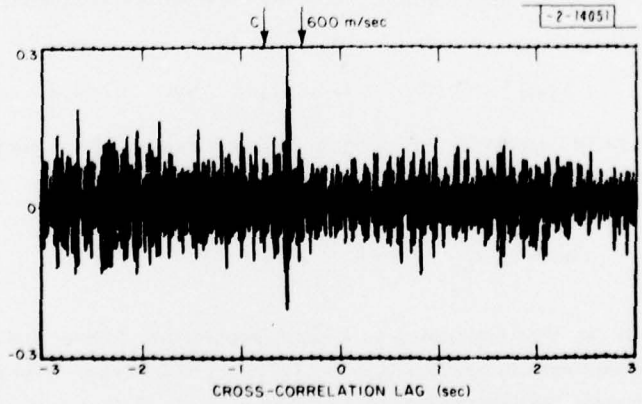

Fig. II-A-9. Cross-correlation of GRA-GRD for A-7 signal. Station separation of 600 m.

B. ACOUSTIC COMPUTATIONAL SIZING

The current concept for an acoustic sensor in a DSN is that each sensor site will include a small array of microphones. Many such sensor sites will be distributed over the area of interest. Each small array will consist of several microphones situated within an aperture of a few meters. A considerable amount of processing must be performed on the raw acoustic data at each small array to detect and calculate an initial estimate of the apparent azimuth of incoming acoustic signals. It is important to estimate the computational requirements (speed and memory) of this front-end processing to see if a hardware configuration that fulfills the requirements is feasible, and, if it is, to estimate the size, nature, and complexity of the hardware that might be deployed in the field with the acoustic arrays. Multisite detection and tracking, signature analyses, or knowledge-based interpretation of data are not considered in the sizing results reported.

1. Strawman Algorithms

Three illustrative strawman algorithms were chosen for the sizing. The computation requirements of these algorithms are typical of those that would be used in a front-end processor for acoustic sensors. The three algorithms have been named (a) Incoherent Frequency-Domain Detection, (b) Coherent Frequency-Domain Detection or Frequency-Domain Beamforming, and (c) Time-Domain Beamforming. The first algorithm only detects the presence of targets, while the latter two algorithms detect and also calculate a rough azimuth for each target. Frequency-Domain Beamforming is a variation of the frequency-wavenumber processing we have used to analyze small array data from our Fort Huachuca experiment. The strawman algorithms are briefly defined below. In each case the input data are N-point sampled waveforms from each of M sensors:

$$\{x_i(n)\} \qquad \text{for } i = 1, 2, \ldots, M \quad \text{and} \quad n = 1, 2, \ldots, N \quad .$$

a. Incoherent Frequency-Domain Detection (Target Detection Only)

(1) Fourier transform each of the waveforms:

$$x_i(n) \Longrightarrow X_i(n) \quad .$$

(2) Calculate the magnitude squared of all the positive-frequency components of the spectrum:

$$|X_i(n)|^2 \qquad \text{for } i = 1, 2, \ldots, M \quad \text{and} \quad n = 1, 2, \ldots, N/2 \quad .$$

(3) Average the spectrum components for each positive frequency over the M sensors of the array:

$$Y(n) = \frac{1}{M} \sum_{i=1}^{M} |X_i(n)|^2 \quad .$$

(4) Smooth the Y values using an s-point rectangular kernel and resample in frequency at a lower rate to obtain $Z(q)$, $q = 1, 2, \ldots, N/2r$ where r is the decimation factor for resampling the smoothed spectrum.

(5) Update the long-term time average of power at each resampled frequency using a single-pole recursive filter which results in exponential weighting of past values in the average:

$$W(q) = cW(q) + Z(q) \qquad \text{for } q = 1, 2, \ldots, N/2r \quad .$$

(6) Calculate a detection statistic:

$$D = \sum_{q=1}^{N/2r} Z(q)/W(q) \quad .$$

When the detection statistic exceeds a threshold, a target is declared to be present. This particular detection statistic is just the sum of detection statistics for each of the frequencies. The development of actual practical algorithms to declare detections based upon the individual detection statistics is an area for serious future research. We expect that actual detection algorithms may become quite complex and involve many heuristics. This also is true of the other detection algorithms described in the following sections.

b. Coherent Frequency-Domain Detection (Frequency-Domain Beamforming)

(1) Fourier transform the waveforms:

$$x_i(n) \Longrightarrow X_i(n) \quad .$$

(2) Calculate a power estimate P_{jk} for each azimuth k and for each frequency j under consideration. This is done using precalculated steering vectors G_{jk}. Steering vectors are complex vectors whose elements G_{jki} represent the phase delay required to align the signal for a particular frequency j, azimuth k, and sensor i with the signal from other sensors. The calculation is:

$$P_{jk} = \sum_{i=1}^{M} G_{jki} X_i(j) \quad .$$

The number of azimuths is a function of frequency and is selected to give overlap in array beams at the 3-dB points. The number of azimuths used for calculation was $2\pi fR/C$ where f is frequency, R is the diameter of the acoustic array, and C is the speed of sound. Only the Q frequencies in a preselected band from f_{min} to f_{max} are considered. The number of azimuths of interest at the highest frequency is V.

(3) Smooth power estimates in frequency using an s-point rectangular smoothing kernel. Resample the smoothed power estimates saving every r^{th} frequency point. This smoothing is done with fixed azimuth. Since the number of azimuths is a function of frequency, we cannot exactly do the frequency smoothing for fixed azimuth but we can do it approximately provided the smoothing kernel is not too broad in frequency. The resulting quantities are Z_{qm} where q goes from 1 to Q/r and for each q, m goes from 1 to the number of azimuths considered at the frequency corresponding to q.

(4) Take long-term averages of the smoothed and resampled power estimates using a single-pole recursive filter:

$$W_{qm} = cW_{qm} + Z_{qm} \quad .$$

(5) Calculate detection statistics corresponding to each of the V azimuths of interest at the highest frequency of interest:

$$D_v = \sum_{q=1}^{q=Q/r} \frac{P_{qm(q,v)}}{W_{qm(q,v)}}$$

where m(q, v) indicates the azimuth index which at frequency q (more precisely the frequency corresponding to index q) corresponds to the azimuth closest to azimuth v (more precisely the azimuth corresponding to index v). When a detection statistic exceeds a threshold, a target is declared at the v^{th} azimuth. As noted previously, the definition and use of actual detection statistics is a matter for serious future research.

c. Time-Domain Beamforming

(1) Beamform in the time domain; that is, add the waveforms from the M sensors with appropriate delays to form V (see Table II-2) beams of N points each. Each beam represents the acoustic signals propagating through the array from a different azimuth:

$$x_i(n) \quad , \quad i = 1, 2, \ldots, M \quad , \quad n = 1, 2, \ldots, N$$

$$\Longrightarrow \qquad y_v(n) \quad , \quad v = 1, 2, \ldots, V \quad , \quad n = 1, 2, \ldots, N \quad .$$

TABLE II-2

SENSOR CONFIGURATION AND PROCESSING REQUIREMENTS FOR STRAWMAN-ALGORITHM SIZING

M = 7 sensors
N = 512 waveform samples from each sensor per second
R = 3 m (diameter of sensor array)
f_{max} = 200 Hz (maximum frequency of interest)
f_{min} = 5 Hz (minimum frequency of interest)
Q = 196 frequencies of interest in algorithm b
r = 10 (frequency resampling interval)
s = 10 (length of frequency smoothing kernel)
V = 20 beams (the number of resolvable beams at f_{max} which is $2\pi f_{max} R/c = 11.4$, where c is the speed of sound)

TABLE II-3

COMPUTATIONAL REQUIREMENTS FOR STRAWMAN ALGORITHMS

a. Incoherent Frequency-Domain Detection (Target Detection Only)

SPEED: ~250,000 operations/second; PROGRAM AND DATA STORAGE: 8K to 16K 16-bit words

$$\underbrace{\frac{MN}{4}(\log_2 N)(24)(1.15)}_{\text{FFT}} + \underbrace{\frac{9MN}{2}}_{\substack{\text{Magnitude}\\ \text{Squared}}} + \underbrace{\frac{MN}{2} + 12}_{\text{Average}} + \underbrace{\frac{N}{2}\frac{(5s-1)}{r}}_{\substack{\text{Smooth and}\\ \text{Resample}}} + \underbrace{\frac{5N}{2r}}_{\substack{\text{Average in}\\ \text{Time}}} + \underbrace{\frac{13N}{2r}}_{\text{Detection}}$$

FFT	Magnitude Squared	Average	Smooth and Resample	Average in Time	Detection
91.89%	6.66%	0.74%	0.52%	0.05%	0.14%

b. Coherent Frequency-Domain Detection (Frequency-Domain Beamforming)

SPEED: ~425,000 operations/second; PROGRAM AND DATA STORAGE: 56K to 64K 16-bit words

$$\underbrace{\frac{MN}{4}(\log_2 N)(24)(1.15)}_{\text{FFT}} + \underbrace{\frac{2\pi f_{avg}}{c}\,RQM\,(20)}_{\substack{\text{Calculation of}\\ P_{ik}}} + \underbrace{VQ\,\frac{(5s-1)}{r}}_{\substack{\text{Smooth and}\\ \text{Resample}}} + \underbrace{VQ\,\frac{5}{r}}_{\text{Average}} + \underbrace{VQ\,\frac{13}{r}}_{\text{Detection}}$$

FFT	Calculation of P_{ik}	Smooth and Resample	Average	Detection
54.42%	39.15%	4.70%	0.48%	1.25%

c. Time-Domain Beamforming

SPEED: ~825,000 operations/second; PROGRAM AND DATA STORAGE: 8K to 16K 16-bit words

$$\underbrace{MNV}_{\text{Beamform}} + \underbrace{\frac{VN}{4}(\log_2 N)(24)(1.15)}_{\text{FFT}} + \underbrace{\frac{9VN}{2}}_{\substack{\text{Magnitude}\\ \text{Squared}}} + \underbrace{\frac{VN\,(5s-1)}{2r}}_{\substack{\text{Smooth and}\\ \text{Resample}}} + \underbrace{\frac{VN5}{2r}}_{\text{Average}} + \underbrace{\frac{VN}{2r}(13)}_{\text{Detection}}$$

Beamform	FFT	Magnitude Squared	Smooth and Resample	Average	Detection
9.10%	80.70%	5.85%	3.18%	0.32%	0.85%

(2) Fourier transform each beam:

$$y_v(n) \Longrightarrow Y_v(n) \quad .$$

(3) Calculate the magnitude squared of the positive frequency components of the spectrum for each beam as was done in step (2) of algorithm a. for each of the individual channels.

(4) Smooth and resample each beam as done for the array average powers in step (4) of algorithm a.

(5) Update the long-term averages for each beam using the same single-pole recursive filter as in step (5) of algorithm a. for each beam spectrum.

(6) Calculate detection statistics for each beam which are equivalent in computation to that used in step (6) of algorithm a. When a detection statistic exceeds a threshold, a target is declared to be present at the azimuth of that beam.

To size and compare the computational requirements of the three algorithms, the sensor configuration and processing requirements described in Table II-2 are utilized. The assumptions made about the processor are:

- All computations are done with 16-bit integer arithmetic.
- An addition or subtraction requires one operation or instruction epoch.
- A multiplication requires four of these epochs.
- A division requires twelve epochs.
- Input data are double-buffered. Thus, the time required for reading the data is assumed to overlap with processing time.
- All calculations are done on the acoustic data for all the sensors in the array once every second.

2. Results

The major results (the number of operations per second and storage requirements for program and data) as well as the breakdown of the various computational tasks are shown in Table II-3. The formula for the number of operations to compute the fast Fourier transform assumes that an N/2-point complex FFT can be done on N real data points. It is also assumed that a complex butterfly requires 24 operation epochs (4 multiplies and 8 additions) and that 15-percent overhead is required for bit-reversal, shuffling of the data, and other details.

The first algorithm, target detection only, can be performed within the given time constraints with a medium-sized minicomputer such as the PDP 11/34. However, the second two algorithms would seriously tax or exceed such a minicomputer's computational capacity. Thus, a medium-sized minicomputer alone would not be sufficient for a front-end processor in an acoustic array.

A significant fact is that in all three algorithms, the major fraction of computational time is spent performing the FFT: 92 percent of the instructions in algorithm a., 54 percent in b., and 80 percent in c. A relatively fast array processor (with approximate maximum FFT computational capacity of a 256 complex-point FFT in 5 msec) could significantly alleviate the processing load on a front-end central computer.

An example of a system that could easily handle the processing requirements of all the algorithms is shown in Fig. II-B-1. This system does not necessarily represent the configuration that would be used at a node in a DSN in the field, but rather represents a research vehicle that could be used to further develop and refine acoustic-sensor detection and location algorithms. The implementation includes a packet radio for communication, a minicomputer (the PDP 11/34), disk storage (for program and data storage), a signal processor, and analog-to-digital converters. The configuration has significant reserve capacity such that a wide variety of computational options could be explored.

The processor shown in Fig. II-B-1 is the Lincoln Digital Signal Processor (LDSP) which is capable of 20-million instructions per second, but has a data-storage capacity of only 4,096 16-bit words and a program-storage capacity of 2,048 16-bit words. However, using current memory technologies, an LDSP-type processor can be designed with more data storage (for example, 65,536 16-bit words) with a small sacrifice in speed – a factor of 2 or 3. While acoustic target detection algorithms alone do not require such a sophisticated fast processor, one might be appropriate to perform processing for several different types of sensors in one area (for example, small radars, infrared, and acoustic sensors). There are other less-sophisticated and less-expensive processors, including those using recently developed charge-coupled-device (CCD) technologies, that are currently available and can be investigated for this application.

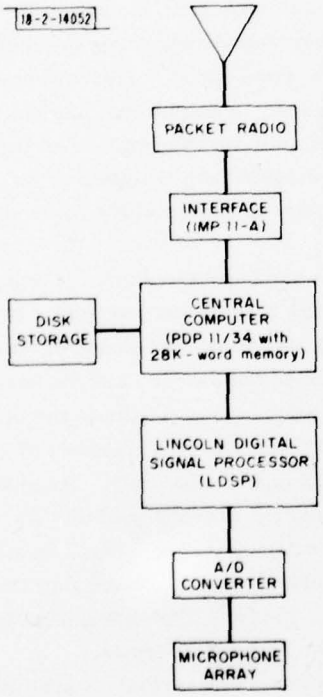

Fig. II-B-1. Acoustic-sensor site.

C. PACKET RADIO AS A RADAR SENSOR

In order for a Packet Radio Net (PRN) to provide digital communication among a set of widely scattered ground terminals [some pairs of which are beyond line-of-sight (LOS)], the packet radios would have to be deployed fairly uniformly over the area, with spacings limited to keep nearest neighbors within LOS. Depending on terrain, foliage, and siting, radio spacings would vary from a few to perhaps as much as 20 km. A relatively uniform grid of radios would provide multiple connectivity for each radio and allow for a reliable adaptable communication system. A similar geographic deployment of radar sensors would also provide good low-altitude coverage for detection of low-flying aircraft and cruise missiles. We report here the results of a study to assess the feasibility of modifying or evolving the packet radios to function as radar sensors, as well as communication terminals.

1. Distributed Radar Sensor Net Options

The packet radio communication waveforms themselves are well suited to accurate time-of-arrival (TOA) measurement, which is needed for bit synchronization to decode a packet. This TOA measurement capability will also be used in a later version of a PRN to provide for automatic position location of terminals. The TOA measurement made on a packet signal reflected from an airborne target would provide a measure of target range. The range resolution provided by the Upgraded Packet Radio (UPR) waveform would be on the order of 3 m. The simplest radar sensor might thus be an omnidirectional UPR which measures only range delay of targets. Monostatic (transmission and reception of target signals at the same site) or bistatic radar modes would both be useful. Range-delay measurements from three omni-sensors would be required to obtain a target-location estimate in three dimensions. This implies a need for overlapping coverage areas of adjacent sensors. Of course, a directional antenna could also be employed for the radar function to provide range and azimuth information on targets as a conventional radar does, but this option entails a more-significant evolution of the UPR. Both monostatic and bistatic ranging sensors have been considered in this study, as well as omnidirectional and narrow-beam antennas.

Although the UPR signal is modulated by data and a bandspreading key, it is possible, at least in principle, to process a data packet with arbitrary modulation and detect the presence of a doppler-shifted signal due to a moving target. One way to do this would be to square the received signals, producing phase-coherent pulses at twice the "mark" and "space" frequencies of the original MSK signal. Filtering would have to be employed to separate the direct path signal from the reflected (doppler-shifted) signal for target detection. This mode of operation is more analogous to that of a CW radar measuring doppler information only. A packet transmission of 10 msec would allow a maximum (theoretical) doppler resolution of 100 Hz, which at the UPR frequency of 1.8 GHz corresponds to a doppler velocity of 16.7 m/sec. Practically achievable doppler resolution would be poorer. The best doppler resolution must also be a small fraction of the maximum doppler caused by a moving target, implying that useful doppler information may be achievable with targets moving 200 m/sec or more (390 knots).

As an alternative to processing the packet-data-transmission format, a special CW signal could also be transmitted somewhere in the UPR band to be used as a CW radar signal. The simplest form of doppler-only sensor is again the omnidirectional sensor which could measure a doppler-vs-time profile for a target. For targets with constant but unknown velocity, three

such doppler-vs-time profiles are needed for a target-track estimate in three dimensions. As in the consideration of ranging sensors, both monostatic and bistatic doppler-only sensors are considered as well as omnidirectional and narrow-beam antennas.

In summary, the set of options considered in this study may be described as follows:

Measurements	Range vs doppler-only
Mode	Monostatic vs bistatic
Antenna	Omnidirectional vs narrow beam
Waveform	UPR waveform vs special waveforms

Considering the bistatic mode antenna options to give four separate cases, a total of 24 sensor options have been considered in this study.

2. Target Model

The targets of interest to a distributed UPR sensor net are low-flying aircraft and cruise missiles. For baseline calculations the fighter-aircraft target is considered first, since cruise missiles are smaller and will be harder to detect. Figure II-C-1 shows the monostatic radar cross section (RCS) of a jet fighter aircraft in a straight and level attitude with the radar in the azimuth plane. The nose-on RCS is generally the lowest, presenting the most difficult detection situation. RCS measurements indicate that jet fighter aircraft typically present between 5- and 10-dBsm RCS in the nose-on sector at the UPR frequency. The target model adopted for baseline calculations in this study is 10 dBsm, which is considerably larger than would be expected for nose-on views of cruise missiles.

Fighter aircraft attempting to penetrate enemy air defenses at low altitudes would probably not exceed speeds of Mach 1 or accelerations of 4 to 6 G's.

3. Baseline SNR Calculations

The following power budget assumes UPR parameters and a 10-dBsm target 10 km from transmitter and receiver (1.8-GHz frequency).

Transmitter power (10 W)	=	10 dBW
Transmit antenna gain	=	9 dB
Path loss outbound (10 km)	=	−117.5 dB
Target gain $4\pi\sigma/\lambda^2$ (10 dBsm)	=	36.5 dB
Path loss inbound (10 km)	=	−117.5 dB
Receive antenna gain	=	9 dBI
Received signal power	=	−170.5 dBW

For an 8-dB noise-figure receiver, the noise power density is $N_o = -196$ dBW/Hz. Thus, for a single 10-μsec UPR pulse, the SNR is

$$E_p/N_o = -170.5 \text{ dBW} - 50 \text{ dB sec} + 196 \text{ dBW/Hz} = -24.5 \text{ dB} \quad .$$

Since an SNR of at least +10 dB is required for detection, the above calculation indicates that a 35-dB improvement in SNR is required beyond the omnidirection UPR parameters to detect a 10-dBsm target at 10 km with a single 10-μsec pulse.

Monostatic and bistatic coverage areas consistent with the 10-km target range from transmitter and receiver are shown in Fig. II-C-2. Overlapping coverage areas require sensor spacings of 10 km or less.

The SNR improvement options are:

(a) Increased transmitter power,
(b) Lower noise receiver front end,
(c) Longer coherent integration time,
(d) Antenna gain, transmit and/or receive.

The transmitter power obtainable from a solid-state transmitter at 1.8 GHz is currently limited to a few hundred watts (average). The receiver noise figure could be reduced to about 3 dB with a new FET front end. Thus, an improved solid-state transmitter (say 300 W) and front end could provide 20 dB of the required 35-dB SNR improvement. In an omni-sensor, the remaining 15 dB of improvement would have to be obtained by extending the coherent integration time to at least 300 μsec.

A modest directional-beam antenna (10° azimuth beamwidth) could provide a mainbeam gain of about 10 dB more than the omnidirectional UPR antenna. Directional antennas on both transmit and receive could thus provide 20 dB of SNR improvement which, together with the improved transmitter and receiver, would allow detection of the desired target with a single 10-μsec pulse.

Thus, there are means available to provide adequate SNR for the aircraft targets of interest at reasonable detection ranges. However, there are other complicating factors which must be considered beyond the SNR, some of which are:

(a) Coherent integration of doppler-shifted signals,
(b) Ground clutter,
(c) Jamming,
(d) Compatibility of directional antennas with UPR channel access protocol.

4. Jamming

Because the received power from a target varies as the fourth power of the target range, a radar is much more vulnerable to jamming than a communication link. Figure II-C-3 shows a plot of jamming-to-signal ratio (JSR) for an omnidirectional sensor receiver vs target range for various ratios of jammer to radar transmitter effective radiated power (ERP). This plot shows that even for modest jammer ERPs (relative to UPR), the JSR requires more improvement than the SNR for the UPR used as a radar sensor. It is important to note that a single airborne jammer at a reasonable standoff range would be able to simultaneously disrupt many omnidirectional radar sensors spread out over a wide area. We concluded that all sensor options which include omnidirectional receivers are thus infeasible because of the vulnerability to a single airborne jammer.

5. Transmitter/Receiver Isolation

A radar which transmits a signal of sufficiently long duration to overlap the received echo signal from a target requires isolation of the transmitter from the receiver. A ranging sensor using a long-duration coded waveform (like the UPR packet waveform) would require suppression of the transmitted signal sufficiently to reduce the correlation sidelobes of the transmitted signal below that of the correlation peak of the target echo. A CW doppler sensor would require transmitter suppression sufficient to reduce the spectral sidelobes of the transmitted signal

below that of the spectral peak of the target echo. For a monostatic radar using a single antenna for transmit and receive, the transmitter-power-to-received-echo-power ratio (TER) at the antenna port would be 180 dB for a 10-dBsm target at 10 km. In this case, it is not feasible to obtain enough transmitter suppression to detect the target signal. This rules out the monostatic radar options using nonpulsed signals (i.e., those options using the UPR packet waveform or a CW signal for doppler estimation).

A significant amount of transmitter-receiver isolation can be realized by employing separate transmit and receive antennas, which really amounts to a bistatic radar mode. The case of a monostatic radar using separate but closely spaced antennas has therefore not been treated as a separate case.

An omni-bistatic radar with transmitter and receiver separation of 10 km will experience a TER of 80 dB. The correlation sidelobes of a ranging sensor using a nonpulsed coded waveform such as the packet waveform could only be a maximum of 60 dB below the correlation peak for an ideal coded waveform extending to the maximum coherent-integration limit of 10 msec. Practical levels of correlation sidelobes are more on the order of 30 to 40 dB, putting the correlation peak of a radar echo 40 to 50 dB below the sidelobes of the direct signal. The only practical bistatic ranging radar option that uses an extended waveform would be one employing directional antennas on both transmitter and receiver. The direct-path signal would then be suppressed by the main-beam-to-sidelobe-gain ratio of both antennas, which could be on the order of 30 dB per antenna. The correlation sidelobes of the direct signal need then be only 30 dB below the correlation peak to allow detection of the desired target.

A CW doppler-only bistatic radar will have to utilize the maximum possible coherent integration time (10 msec) in order to achieve the desired doppler resolution (100 Hz). This implies that the direct-path signal must be suppressed sufficiently to reduce the near-in spectral sidelobes of the direct signal below the spectral peak of a target echo. For the minimum separation in frequency of 100 Hz between the direct-path signal and a doppler-shifted echo, it would be difficult but possible to suppress the direct signal relative to the echo as much as 60 dB under ideal conditions. Thus, the only bistatic doppler-only radar option that appears practically feasible is also one employing directional antennas on both transmitter and receiver.

In summary, transmitter-receiver isolation for radar modes using long-duration signals which would overlap received echoes is a very significant factor which eliminates many of the radar options.

6. Summary and Conclusions

Table II-4 lists the twelve ranging-sensor options that were considered in this study. The table shows that jamming vulnerability and the transmitter-receiver isolation requirements taken together eliminate all but four of the options. Table II-5 lists the twelve CW doppler-only sensor options studied. Jamming eliminates all options using the UPR waveform because the operation of all radars on a common carrier frequency increases the jamming vulnerability of the set of sensors. The transmitter-receiver isolation requirements also eliminate an additional number of options, resulting in only one surviving option. The surviving options are listed in Table II-6 in order of increasing difficulty of implementation. It appears that the changes required to evolve packet radios into practical radar sensors would be very major. Moreover, the detection of low-flying aircraft and cruise missiles is a difficult sensor problem, even with no constraints upon the sensor design. Rather than try to evolve packet radios into a radar sensor, we recommend that a small radar sensor be developed to be colocated with packet radios in a DSN.

TABLE II-4

RANGING-SENSOR OPTIONS TREE
(Feasible Options Marked With ●)

Mode	Transmit Antenna	Receive Antenna	Waveform	ECM Vulnerability	Direct-Path Suppression (dB)	Required SNR Improvement (dB)	
Monostatic	Omni	Omni	UPR	Severe	190	35	
			Special	Severe	Pulsed	35	
	Narrow Beam	Narrow Beam	UPR	Operable	190	15	
			Special	Operable	Pulsed	15	●
Bistatic	Omni	Omni	UPR	Severe	90	35	
			Special	Severe	Pulsed	35	
		Narrow Beam	UPR	Moderate	60	25	
			Special	Moderate	Pulsed	25	●
	Narrow Beam	Omni	UPR	Severe	60	25	
			Special	Severe	Pulsed	25	
		Narrow Beam	UPR	Operable	30	15	●
			Special	Operable	Pulsed	15	●

TABLE II-5

DOPPLER-ONLY (CW) SENSOR OPTIONS TREE
(Feasible Option Marked With ●)

Mode	Transmit Antenna	Receive Antenna	Waveform	ECM Vulnerability	Direct-Path Suppression (dB)	Required SNR Improvement (dB)
Monostatic	Omni	Omni	UPR	Severe	190	35
			Special	Severe	190	35
	Narrow Beam	Narrow Beam	UPR	Severe	190	15
			Special	Operable	190	15
Bistatic	Omni	Omni	UPR	Severe	90	35
			Special	Severe	90	35
		Narrow Beam	UPR	Severe	60	25
			Special	Moderate	60	25
	Narrow Beam	Omni	UPR	Severe	60	25
			Special	Severe	60	25
		Narrow Beam	UPR	Severe	30	15
			Special	Operable	30	15 ●

TABLE II-6

CHARACTERISTICS OF SURVIVING UPR RADAR-SENSOR OPTIONS

Type	Mode	Transmit Antenna	Receive Antenna	Waveform	Direct Path Suppression Required (dB)	SNR Improvement Required (dB)	New Transmitter/ Receiver?	Coherent Integration Required (μsec)	Estimated Clutter Suppression Required (dB)
Ranging	Monostatic	Narrow Beam	Narrow Beam	Pulse Train	NA†	15	No	300	20
Ranging	Bistatic	Omni	Narrow Beam	Pulse Train	NA†	25	Yes	100	25
Ranging	Bistatic	Narrow Beam	Narrow Beam	Pulse Train	NA†	15	No	300	15
Ranging	Bistatic	Narrow Beam	Narrow Beam	UPR Signal	30	15	Yes	10	15
Doppler-Only	Bistatic	Narrow Beam	Narrow Beam	CW Signal	30	15	No	10,000‡	NA

† Transmitter/receiver isolation achieved by pulsed waveforms.

‡ Maximum feasible coherent integration time is dictated by required doppler resolution.

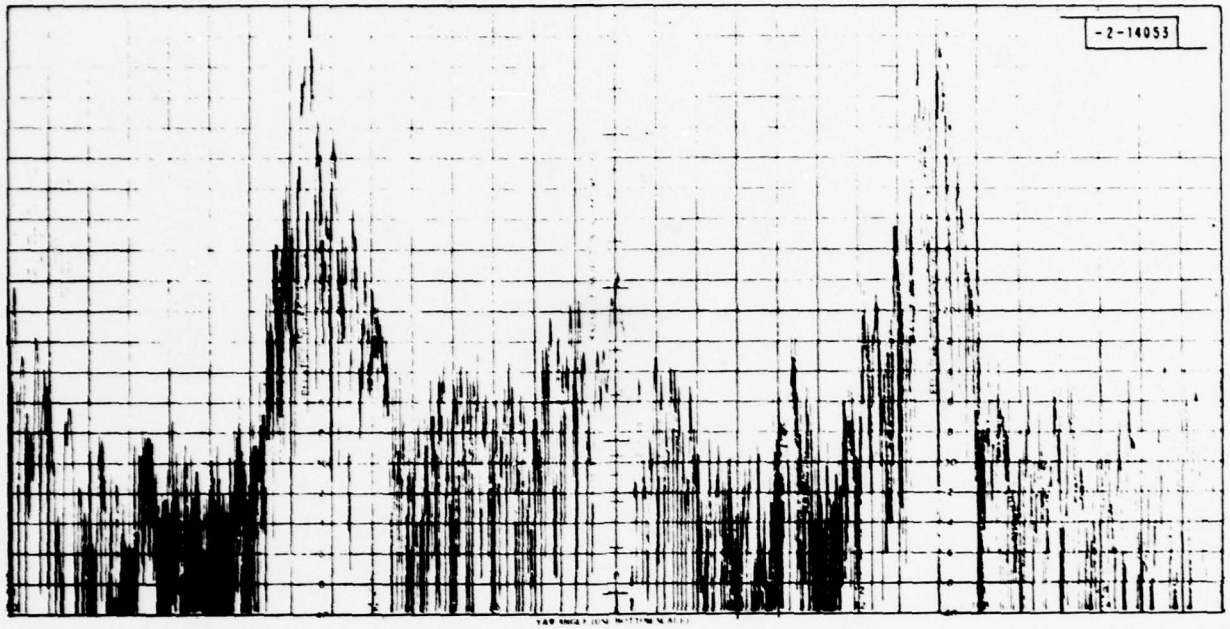

Fig. II-C-1. Horizontal plane monostatic radar cross section of typical jet fighter (vertical polarization, 3 GHz).

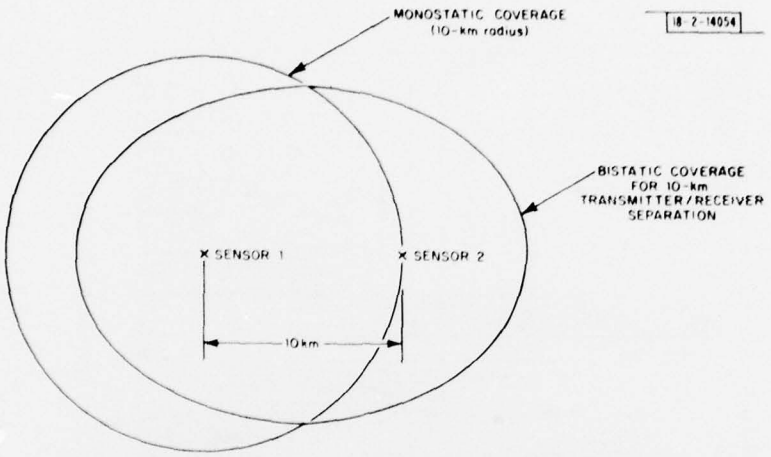

Fig. II-C-2. Coverage by monostatic and bistatic radar modes for $R_1 \cdot R_2 = 100\ km^2$.

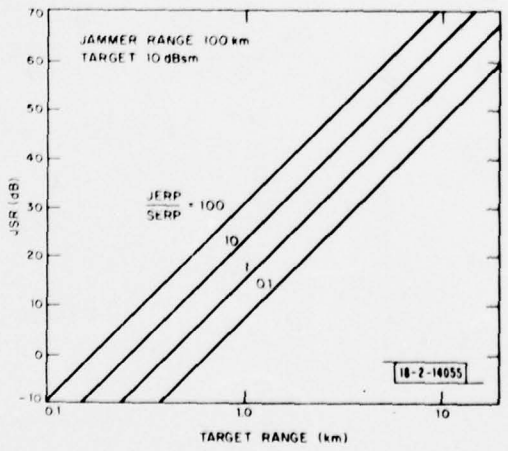

Fig. II-C-3. UPR radar sensor JSR.

D. SEARCH-MODE PASSIVE IR FOR LOW-FLYING AIRCRAFT

In this section, we examine the use of IR detectors in the context of a DSN whose objective is to detect and track low-flying aircraft. In the spirit of our previous acoustic investigations, we restrict the sensor to be passive in its basic mode of operation and to be capable of unattended operation. The problem naturally divides itself into three areas: (1) sources and background noise that might obscure or be misidentified as sources, (2) source-receiver path effects, and (3) receiver characteristics. The basic questions we wish to answer are what can be detected and at what distance can detection be made. Here, we will try to answer these questions by examining the basic engineering principles of IR in the context of a specific example.

Detection range, target, path, and detector characteristics are related through the range equation[2]

$$\frac{W_\lambda}{\pi R^2} t_a \approx \frac{4\Omega^{1/2}}{\pi D D^* t_o \sqrt{NT}} SNR$$

where

W_λ = Source power in the band of interest,

R = Detection range,

t_a = Loss in the atmosphere,

Ω = Total solid angle scanned,

D = Diameter of the optics,

D^* = Detectivity of the sensor,

t_o = Loss due to optics,

N = Number of detectors,

T = Time to scan Ω, and

SNR = Signal-to-noise ratio required for a given probability of detection.

The term on the left-hand side is the power flux that arrives at the optics due to a source at distance R. The left-hand side describes the power flux required at the aperture to match the detector-optics system noise multiplied by the SNR that will produce the desired confidence level for detection.

Airborne targets emit energy above normal background levels from the heated skin, hot engine parts, and hot exhaust gases. Generally, each of these sources has different radiation characteristics, any one of which might be best for detection purposes depending on the aspect and dynamics of the target, the construction of the vehicle, or atmospheric conditions. The total power flux produced by an object,

$$W = \epsilon \sigma T^4$$

is proportional to the fourth power of its absolute temperature T and its emissivity ϵ, where σ (the Stefan-Boltzmann constant) is $5.67 * 10^{-12}$ W/(cm^2-K^4). At supersonic speeds the hot skin may dominate the radiation, whereas at lower speeds the relative size of the exhaust plume and

hot engine parts, their temperatures, and emissivities determine the proportion of radiation from each. The distribution of radiant power at various wavelengths λ is given by Planck's equation

$$W_\lambda = \epsilon_\lambda C_1 d\lambda / \left(\lambda^5 \{\exp[C_2/(\lambda T)] - 1\}\right)$$

where ϵ_λ is the emissivity at the wavelength λ, and

$$C_1 = 3.75 * 10^{12} \text{ W-cm}^2$$

$$C_2 = 1.438 * 10^4 \text{ } \mu\text{m-K} \quad .$$

For constant emissivity, between room temperature (300 K) and the melting point of steel (2900 K), the peak of the distribution decreases from about 10 to 1 μm spanning the infrared spectrum. Since the atmosphere severely attenuates certain energy bands and since the composition of the exhaust as well as its temperature and shape determine its radiation, an exact statement of source radiation is difficult to make. Generally speaking, the radiation pattern is the superposition of the three effects combined with the shielding effect of the aircraft itself. The result is commonly an order-of-magnitude difference in radiated power at different azimuths and inclination angles. As an example, jet aircraft generally radiate between 100 and 1000 W total power with plume temperatures of about 1000 K (see Ref. 3). If a source is emitting 100 W total, then in a 1-μm band about 2 μm, the power emitted is about 10 W as can be derived from the above equations assuming a 1000 K source. At a distance of 10 km then, the power flux is

$$t_a W_\lambda / \pi R^2 = t_a * 3 * 10^{-11} \text{ W/cm}^2 \quad .$$

The 2-μm band was chosen as an example since plume radiation is strong in the band[4] and for the detector and path considerations that are explained below.

In the lower atmosphere, water and CO_2 severely attenuate the propagation of IR energy. However, conditions exist that allow certain spectral bands of energy to be transmitted over large distances. In the IR region, the bands of transmittance are 8 to 14 μm, 3 to 5 μm, and 0.7 to 2.5 μm (see Ref. 5). In each of these bands, attenuation still exists to the degree of about 0.5 dB/km on the best of days up to many dB/km during rain, fog, or haze conditions. Specifically, near 2 μm, when the visibility is about 10 km the attenuation is about 4 dB/km. At 25-km visibility, the attenuation is about 2 dB/km. Following upon the example above, 4-dB/km attenuation at 10 km leads to a power flux of

$$t_a \frac{W_\lambda}{\pi R^2} = 3 * 10^{-13} \text{ W/cm}^2 \quad .$$

It remains then to examine detectors suitable for DSN applications.

The IR receiver system consists of the optics for collecting and focusing incoming target photons onto a detector that counts them. The instantaneous field of view (IFOV) of the system may be estimated by considering the background noise characteristics that can lead to misidentifying false targets (such as cloud-top reflections) with real targets. For instance, in the 2-μm band the worst background level from sun reflection at the earth's surface will be about 1.5×10^4 W/cm^2-sr (see Ref. 2). Since reflections are diffuse compared with real targets,

discrimination between them will be possible if the IFOV is small compared with the ratio of the target power flux at the aperture to the reflection flux per steradian. For the example, we find

$$\text{IFOV} = \frac{3 * 10^{-13}\ \text{W/cm}^2}{1.5 * 10^{-4}\ \text{W/cm}^2\text{-sr}} = 2 * 10^{9}\ \text{sr}$$

or about 45 μrad on a side, which is about the resolving power of 5-cm circular optics.[6] Thus, a telescope with 5-cm optics or larger is required. The focal depth of the telescope will depend on detector size requirements. If a search is conducted at a single elevation at all azimuths, then the total solid angle scanned will be

$$\Omega = 2\pi * 45 * 10^{-6}\ \text{sr} = 2.8 * 10^{-4}\ \text{sr} \quad .$$

Of course, many elevations could be scanned utilizing a vertical array of sensors. Say, for tracking purposes, that we wish to scan Ω every second (an aircraft traveling near the speed of sound moves about 300 m in 1 sec). Thus, the time t to dwell at each point in the field of view would be

$$t = \frac{2 * 10^{-9}\ \text{sr}}{2.8 * 10^{-4}\ \text{sr}}\ 1\ \text{sec} = 7\ \mu\text{sec} \quad .$$

IR detectors are characterized by their detectivity D* which is extremely dependent on detector temperature, time constant, and spectral response. Given the parameters above, the range equation can be rearranged to study detector characteristics trade-offs. Assuming an optics loss of 0.5 for a 10-cm aperture and a SNR of 5 (this assures 99.9-percent probability of detection in a single scan[2]), we find

$$D^{*}\ (\text{cm/W-sec}^{1/2})\ N^{1/2} = 3.7 * 10^{11}\ \text{cm/(W-sec}^{1/2}) \quad .$$

Table II-7 shows two possible detectors that might be used in a system. An array of four cooled indium antimonide detectors would suffice, while it would take 60×10^{3} lead selenide detectors to accomplish the task. Lead sulfide is a common room-temperature detector with a large detectivity, but it unfortunately has a 250-μsec rise time and is thus unsuitable since the dwell time required for our example is only 7 μsec.

TABLE II-7
IR DETECTOR CHARACTERISTICS

	Type Detector	
	Indium Antimonide	Lead Selenide
D* (cm/W-sec$^{1/2}$)	$2 * 10^{11}$	$1.5 * 10^{9}$
Rise Time (μsec)	0.2	1
Temperature (K)	77	300
Smallest Size (mm^2)	0.01	0.01

The above analysis is not an attempt at a sensor design. What is clear from the above is that low-flying aircraft produce a sufficient photon flux at many kilometer distances to be detected, and therefore IR sensors should be further considered. However, the above also suggests that the system performance requirements for IR sensors may not be met by simple or inexpensive sensors due to cooling or very large detector array fabrication requirements.

III. MULTISITE DETECTION

In the area of multisite detection, the utilization of acoustic azimuth measurements is emphasized. A DSN composed of multiple small acoustic arrays for detection and tracking of low-flying aircraft seems most appropriate for the first stages of a testbed system. It is thus clear that more understanding of the multisite utilization of such acoustic data is called for.

Two complementary efforts were undertaken, and progress is summarized in the following sections. The first was to develop the surveillance space search approach suggested in our previous SATS.[1] In that effort, some basic experimental software has been developed and some initial evaluation has been done for the case of acoustic sensors. Several issues needing further study have been identified. Computational sizing has been deferred until a planned major restructuring of the algorithms is done. The second effort was to develop and evaluate algorithms to directly locate aircraft using azimuth observations from only two acoustic sites measuring azimuth. For this it was assumed that the sensor site could associate a sequence of azimuth observations with a single target so that it actually delivered a time series of azimuth observations already associated with each other.

A. DECISION THEORETIC SURVEILLANCE SPACE SEARCH MULTISITE DETECTION

In this section, we report progress on general algorithms that combine data from several sensor sites to detect and locate targets even when data from a single sensor may not be sufficient to locate a target. This work has been done in the context of acoustic sensors which can measure the acoustic azimuth of targets. For such acoustic sensors the azimuth from which sound is arriving may not correspond to the azimuth at which the target is located. This is a factor which complicates the problem and must be addressed. The approach we evolved can be adapted to a wide variety of sensors without propagation delay problems, and can also handle multiple-sensor types without added difficulty.

The surveillance space search approach to the problem is to divide the physical space of interest into three-dimensional cells (the space covered by the cells may or may not include the location of sensors), and then search the space cell-by-cell for the targets. For the acoustic problem of immediate concern, we assume that the sensors periodically make azimuth measurements, and record the time of the measurement along with the azimuth. We also assume that the sensors are synchronized (to tenths of seconds) with each other and the multisite-detection processor.

The search for targets is made through each cell in the target space at periodic intervals called surveillance times. The search technique is as follows. For each cell, the hypothesis is made that there is a sound-emitting target within the boundaries of the cell at the surveillance time. Given a cell, the data from each sensor covering the surveillance space are considered in turn. The azimuth that each sensor would measure if there were indeed such a target in the cell at the surveillance time, and the time of arrival of this sound at the sensor are calculated. The azimuth and time are actually ranges of azimuth and time because the cell has finite dimensions. This range of azimuth is then compared with those data that the sensor actually measured during the predicted time range. If there is an agreement, a count is listed in this cell for the particular sensor at the surveillance time. Any additional data that the sensor may have, such as if this measurement is consistent with others comprising the track of one particular target,

can also be included with the cell corroboration. When all the cells have been searched, targets are declared in those cells with corroborations from many sensors. The number of corroborations is an ad hoc decision statistic selected for initial studies. When the search is done at several successive surveillance times, targets can be tracked as they move from cell-to-cell.

A significant advantage to this detection approach is that it is not necessary to make any assumptions about the dynamics (the velocity or trajectory) of the target. One only assumes a position in a cell. A disadvantage of such a multisite-detection scheme for acoustic sensors is that the searches must be done at a delay to real time. Since targets are hypothesized in each cell at the surveillance time, one must account for the acoustic travel time of the targets' sound from the cell to the sensor. Thus, the surveillance time or time of the search must be done at a delay equal to the travel time from a cell to the most distant sensor from which one desires azimuthal data.

1. Software

A simulation program of the surveillance space search algorithm has been written in the C programming language to run on a PDP 11. The program consists of three major sections: initialization, search, and report.

In the initialization routines, the position of sensors and the initial positions and velocities of the targets are used to calculate the acoustic azimuths that each sensor measures as the targets pass through the area of interest. Only targets with constant velocity have been used. A rectangular, box-shaped grid of cubed-shaped cells is also set up over the area and altitudes of interest. As a result of these routines, each sensor has a table that includes azimuth measurements taken over the time interval in which the targets passed through the area of interest and the time for each measurement. In the current simulation, it is assumed that all sensors make measurements simultaneously, once a second.

The details of the search routines can be explained with the aid of Fig. III-A-1(a-b). As mentioned above, surveillance space search is done after a delay from the actual real time. The sensor data that are used to corroborate the hypotheses that targets are in the various cells include all those measurements made from the time of the search to the current real time, as indicated in Fig. III-A-1(b). During the search, each cell in the space is checked. Once a cell is chosen, data from each sensor are then considered in turn.

For each cell-sensor combination, two times, t_{min} and t_{max} (those times required for acoustic signals to travel from the closest and farthest boundaries of the cell to the sensor), are first calculated as shown in Fig. III-A-1(a). The two times and the geometrical relationship between the sensor and the surveillance cell provide a mapping of the surveillance space cell into a data space cell in the sensor's measurement space as shown in the figure. If measured azimuths are found in the data space cell, they are said to corroborate the hypothesis that a target is in the surveillance cell at the surveillance time, and this agreement is noted in the surveillance cell along with the sensor number and the time of the measurement(s). In the particular example shown in Fig. III-A-1(a-b), there are two azimuth measurements in one of the data cells because the target remained within the surveillance cell during two measurement periods of the sensor. Another surveillance space cell mapping is shown in the figure. No measurements appear in this second data space cell. When checking if the azimuth measurements fall in the data space cell, the current implementation uses an error margin of plus or minus one-half degree.

After all cells are searched, a list of corroborations can be printed out or the entire grid of cells can be displayed with corroborations noted, as is shown in Figs. III-A-2 through III-A-8 in the sections which follow. Those cells with corroborations from all or nearly all the nearby sensors are considered to very likely have one or more targets in them.

2. Target Detection and Location

Some sample scenarios were run through the simulation. The area of interest consists of a box, 5-km square and 0.5 km high. The box is quantized into 100 cells, each a 0.5-km cube. Five acoustic sensors are distributed over the area, all are at zero altitude. Four sensors are at the corners of the 5-km square area of interest and the fifth is at the center.

a. Static Target

To more easily understand how the algorithm works, a surveillance space search was done for a static target at zero altitude. The search was done after a 20-sec delay, that is, after the sensors had recorded azimuthal data for 20 sec. The corroborations of predicted azimuths and sensor data are shown in Fig. III-A-2(a). A corroboration that a target is in the cell is designated simply by the number of the sensor. As was discussed above, those cells with more than one corroboration from the same sensor simply contain more than one cell-sensor distance, with an acoustic travel time equal to the times that the sensors made measurements. As shown more clearly in Fig. III-A-2(b), the cells with corroborative data from one sensor form a straight line from the sensor through the target. In the figure, straight lines were drawn from the sensors through the target. The corroborations farther from the sensor represent later measurements times. The sensor measures a constant azimuth for 20 sec. Thus, the sensor has an azimuth that agrees with that predicted by cells along the straight line through the target and sensor for acoustic travel times from 0 to 20 sec.

The cell in which all the straight lines intersect contains corroborations from all the sensors and, indeed, also contains the target. For this example, this cell has corroborations from all 5 sensors – a total of 12. Other cells have corroborations from a maximum of 3 different sensors – a maximum total of 4.

b. Moving Target

Detection and location of a target that is moving are more difficult. As the sensors make sequential azimuth measurements, the target is moving and its acoustic azimuth is changing. The resulting line of cells containing corroborations is not straight, as is shown in Fig. III-A-3. In the figure, the cells with one or more corroborations by sensor 0 for possible target locations at time t = 0, using all measurements available for the interval t = 0 to t = 20, have been marked with solid circles. The actual target is traveling in the direction shown at a speed of 174.9 m/sec (M = 0.53) at zero altitude. The target is in the cell marked with an X at t = 0. The acoustic azimuths that sensor 0 measures at t = 0 and 20 sec are also shown in the figure. A curve was drawn by eye through the cells with corroborations.

As with the static target, the cell in which corroborations exist from all sensors is hypothesized to contain the target. Figures III-A-4(a) through (f) show the results of searches at surveillance times, t = 0, 4, 8, 12, 16, and 20 sec, respectively, as real time progresses from t = 20 to 40 sec. Each surveillance search is done with an interval of 20 sec of sensor

TABLE III-1

CORROBORATION SCORES USED TO LOCATE ONE MOVING TARGET

Surveillance Time (sec)	No. of Sensors Corroborating Hypothesis	Total No. of Corroborations
0	5:3	9:4
4	5:3	7:5
8	5:3	8:5
12	5:3	5:4
16	5:2	8:4
20	5:4	8:5

TABLE III-2

CORROBORATION SCORES USED TO LOCATE TWO MOVING TARGETS

Surveillance Time (sec)	No. of Sensors Corroborating Hypothesis		Total No. of Corroborations	
	Target A	Target B	Target A	Target B
0	5:3	5:3	10:6	7:6
4	5:4	5:4	8:6	6:6
8	5:3	4:3	9:7	5:7
12	4:4	4:4	9:6	9:6
16	5:3	5:3	10:6	10:6

data. To avoid cluttered figures, only one corroboration per sensor is indicated in a cell. The cell in which the target was located at the search time (marked with an X in the figure) was corroborated by all 5 sensors at these times.

The scores by which the target was located are presented in Table III-1. The two numbers shown are the number of corroborations in the cell with the target and the maximum number of such corroborations in other cells in the grid.

For this particular example, the cell in which the target was traveling could be identified easily by selecting those cells with corroborations from all sensors. These cells could also be identified by selecting those cells with the maximum total number of corroborations {this technique is a little weak for t = 12 [Fig. III-A-4(d)] where the target is very close to a cell boundary}. As will be seen below, there are examples in which neither of these counting techniques alone can select target cells, but both can be used to select those cells containing targets.

c. *Two Moving Targets*

Is this search technique able to distinguish among several targets traveling through the area of interest? The scenario of Figs. III-A-4(a) through (f) was augmented with a second, faster target traveling at 279.5 m/sec (M = 0.84), and zero altitude. The search algorithm was able to identify definitively two cells with targets for 4 out of the 5 surveillance space searches. The cells in which the targets were located were not always corroborated by all 5 sensors, as shown in Table III-2 and Figs. III-A-5(a-b) through III-A-8(a-b), where the trajectories of the two targets are shown as lines. The locations of the targets at the search time are marked with an X. However, by considering both the number of sensors corroborating each cell and the total number of corroborations for each cell, both target-containing cells were located in the four searches. At t = 8 sec [Fig. III-A-6(a-b)], using the above-mentioned criteria, the faster target is not correctly located and a target is located erroneously in the cells that are shaded in the figure. Using the results of the searches at t = 0, 4, 12, and 16 sec, the assumptions that the targets are moving at constant velocity, and some rudimentary tracking, one can correctly locate the faster target at t = 8 sec. Perhaps surveillance searches done more often could also resolve this problem.

Again, for this example the surveillance space search can detect and locate two cells with targets in the area of interest. The detection and location appear more difficult with two targets, and the question arises as to how often should the surveillance space search be conducted. The nature of the tracking process to be done at a higher level is also brought into consideration.

3. Discussion

The results described above comprise only an initial study of the surveillance space search multisite detection and location algorithm. There are a large number of issues that have been raised in implementing the algorithm.

As presently implemented, the search algorithm is not efficient. All the cells are searched, regardless of the chance of finding targets in them. The above examples use a rather coarse grid – 0.5-km cubes – over a small area. If a larger area and altitude were more finely quantized, it could easily require the task of searching more than one million cells for one surveillance space search. To keep track of several targets, the search might have to be repeated more often. Alternately, using a finer grid (smaller cell dimensions) might reduce the necessity of searching often. Clearly, the computational load increases rapidly with the precision with which one wishes to follow the targets through the area of interest.

Other quantization effects are apparent. Given that acoustic sensors make measurements once a second, a faster target will result in fewer measurements as it travels through the surveillance space. Fewer measurements result in fewer corroborations with the azimuths predicted by the cell-sensor geometries. One possible solution is to interpolate the target's trajectory – that is, interpolate values between measurements and use the interpolated values in the search algorithm. However, the interpolation procedures add to the computational load; also, if there are several targets (several azimuth measurements for one given time), it is not always clear which azimuths should be used for interpolation. An alternative solution is to have the acoustic sensors generate azimuth measurements more often; however, this solution results in a greater computational load for the front-end processors.

Further study is required to better understand the properties of the search algorithm and the utility of its output. For example, the above results have not included the effects of false alarms or noisy azimuth measurements. Would several false azimuths cause the detection and location algorithm to fail? Could a sophisticated tracking algorithm use the results from several inconclusive surveillance space searches and track a target?

Another issue is target altitude. Targets will be at different and perhaps varying altitudes. Can results with satisfactory accuracy be obtained from a search at only one altitude, or must the search be carried out through all the cells of several layers of surveillance space, increasing the computational load? Work reported in Sec. B on p.40 has direct bearing upon these questions.

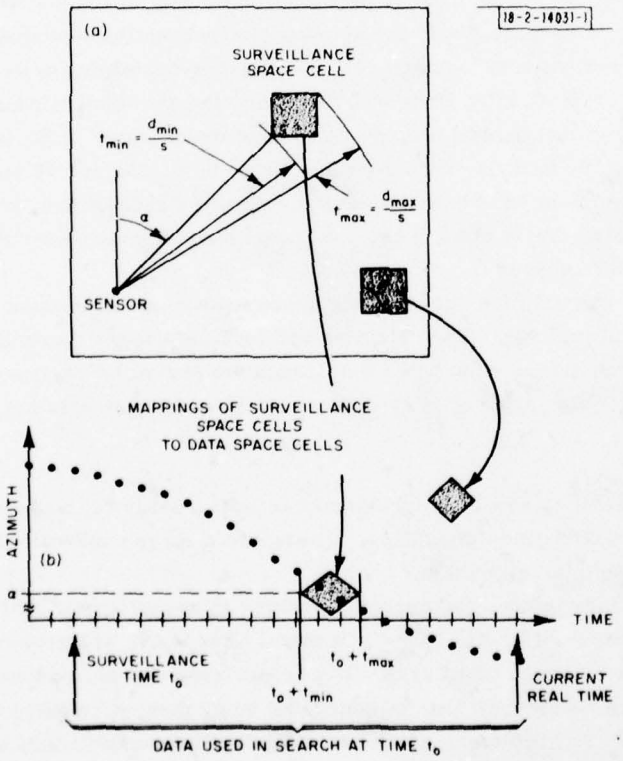

Fig. III-A-1. Multisite detection: surveillance space search. (a) Surveillance space; (b) azimuthal data measured at sensor.

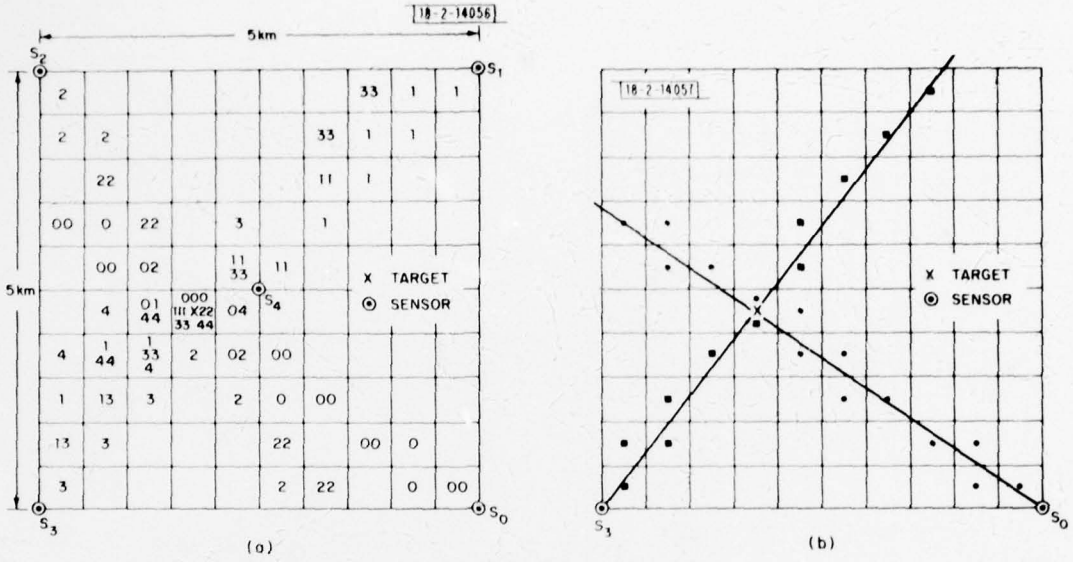

Fig. III-A-2. Static target: (a) all corroborations; (b) corroborations from sensors 0 and 3 only.

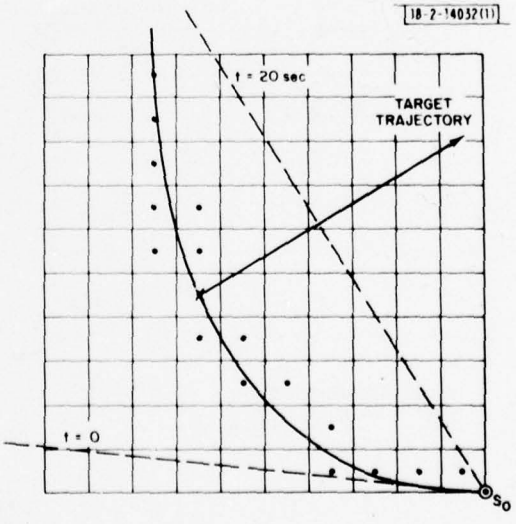

Fig. III-A-3. Corroborations of a single moving target by a single sensor. Solid dots indicate sensor 0 corroborations. Dashed lines show acoustic azimuth of target at times t = 0 and 20 sec. Target location at t = 0 is marked by an X. Target velocity is Mach 0.53. Curved solid line marks locus of corroborated cells.

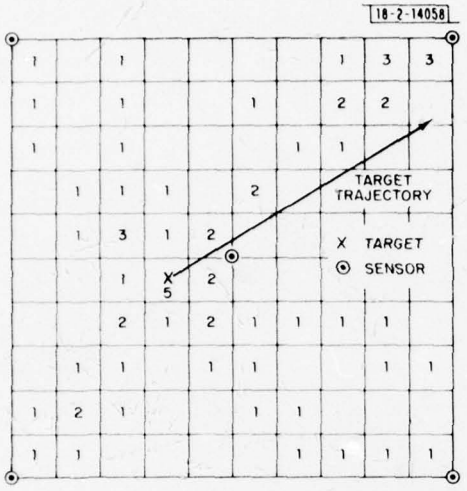

(a) Surveillance time = 0 sec; real time = 20 sec.

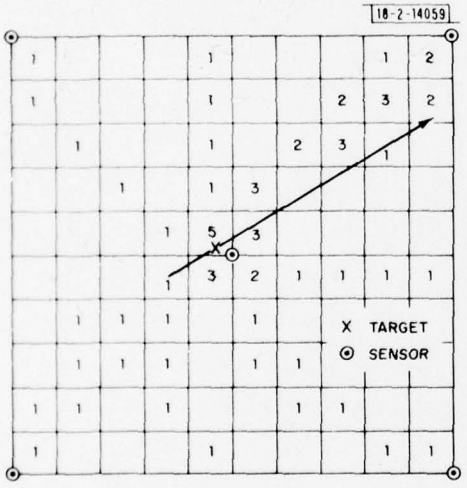

(b) Surveillance time = 4 sec; real time = 24 sec.

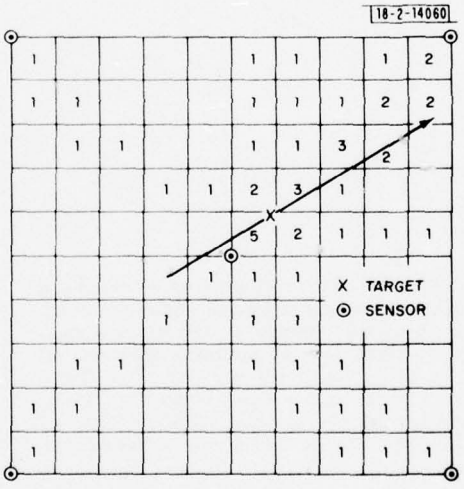

(c) Surveillance time = 8 sec; real time = 28 sec.

Fig. III-A-4(a-f). Number of corroborating sensors. Target moving through surveillance space at 174.9 m/sec. Target location at surveillance time marked by an X.

(d) Surveillance time = 12 sec; real time = 32 sec.

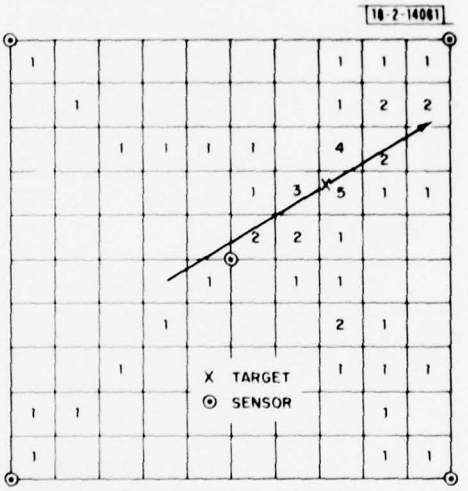

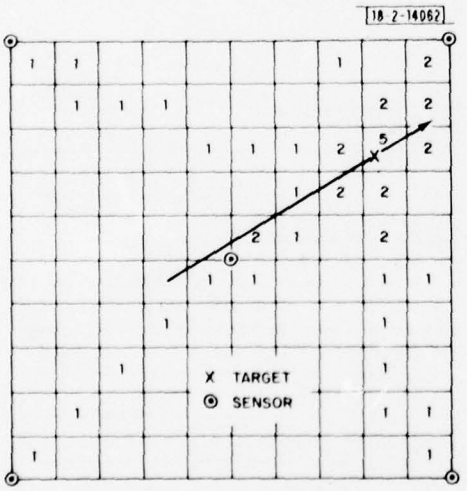

(e) Surveillance time = 16 sec; real time = 36 sec.

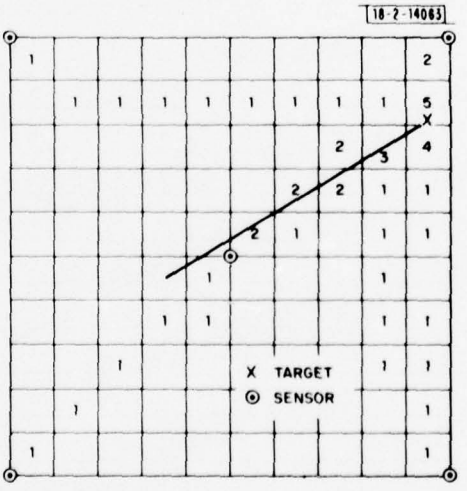

(f) Surveillance time = 20 sec; real time = 40 sec.

Fig. III-A-4(a-f). Continued.

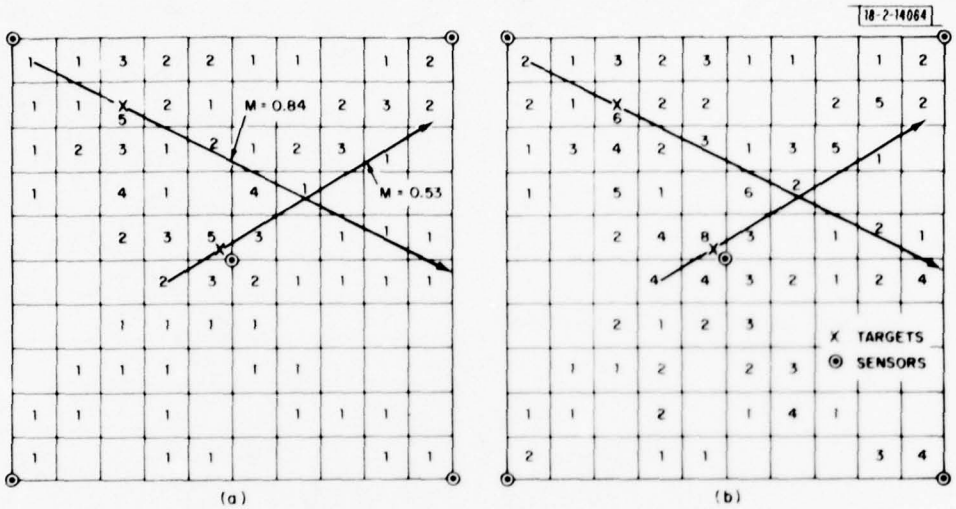

Fig. III-A-5. Two moving targets: surveillance time = 4 sec (real time = 24 sec). (a) Number of corroborating sensors; (b) total number of corroborations.

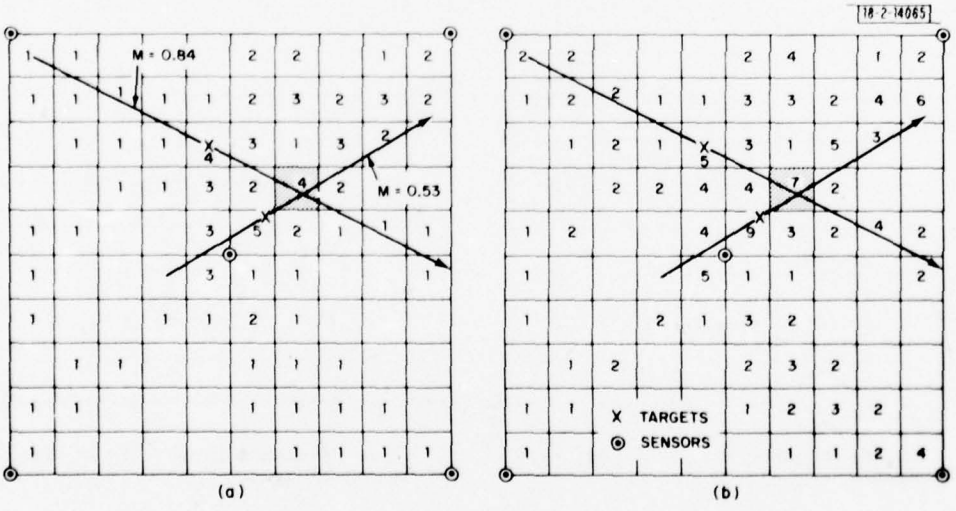

Fig. III-A-6. Two moving targets: surveillance time = 8 sec (real time = 28 sec). (a) Number of corroborating sensors; (b) total number of corroborations.

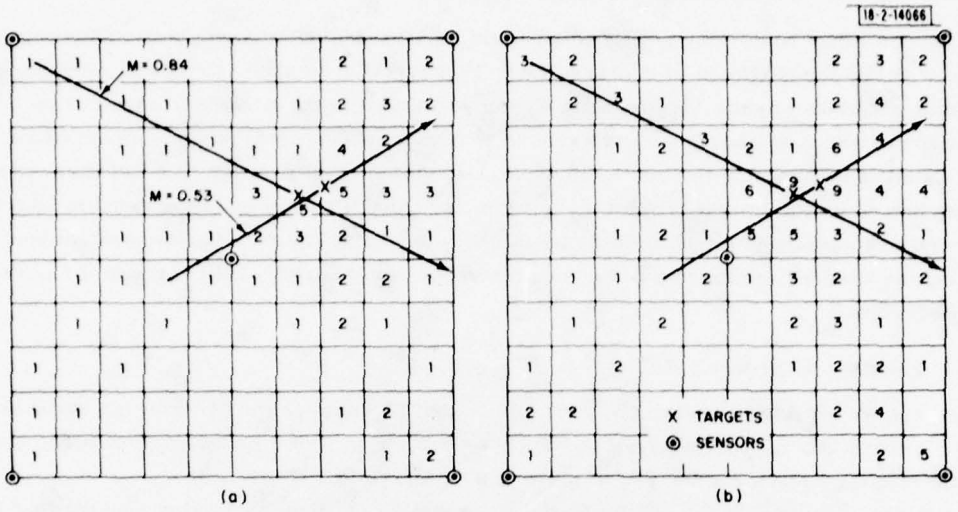

Fig. III-A-7. Two moving targets: surveillance time = 12 sec (real time = 32 sec). (a) Number of corroborating sensors, (b) total number of corroborations.

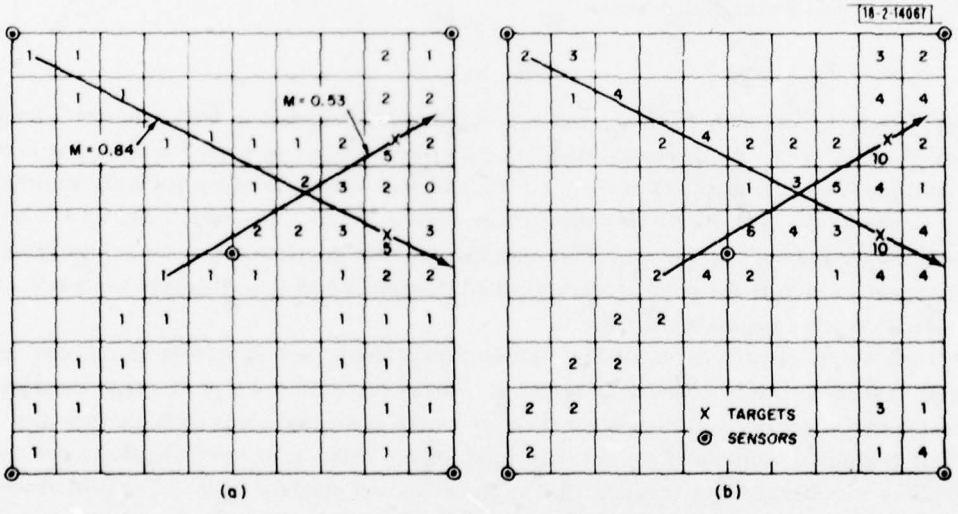

Fig. III-A-8. Two moving targets: surveillance time = 16 sec (real time = 36 sec). (a) Number of corroborating sensors, (b) total number of corroborations.

B. TWO-SENSOR TARGET LOCATION

A second effort to develop multisite acoustic location algorithms has been under way concurrent with the investigation of decision theoretic surveillance space search alternatives. Our immediate goal was to show that an aircraft can be located in the horizontal plane using data from only two acoustic sensors. Each sensor is a microphone array whose outputs are of the form "sound is coming from azimuth (horizontal direction) ϕ at time t." We felt that understanding how to do this might furnish insight into the capabilities of acoustic sensors and that the algorithms developed might actually be of use in a DSN. The two-sensor method described below can be used as an alternative to, supplement to, or theoretical background for surveillance space searching.

1. Locating an Aircraft

Suppose we have two sensors, S_1 and S_2, located 10 km apart and both at the same height, which is zero in our coordinate system. Suppose a plane is flying around somewhere, and the azimuth-vs-time curves for the two sensors are as shown in Fig. III-B-1.

First, we want to find the plane at time t, assuming (with no particular reason) that the plane is at height $z = 0$. Consider just the S_1 data. The sound emitted by the plane at time t must arrive at S_1 at some time $t_1 > t$. Let ϕ_1 be the azimuth reading measured for time t_1. Then, at time t the plane is distance

$$R_1 = (t_1 - t) \cdot (\text{speed of sound})$$

from S_1, or at horizontal distance

$$r_1 = \sqrt{R_1^2 - z^2}$$

from S_1. Given t_1, we have found ϕ_1 and r_1, which specify a point in the horizontal plane. The set of all pairs (r_1, ϕ_1) given by all $t_1 > t$ generates a curve of possible positions in the horizontal plane for the airplane at time t. We call this latter curve the possible position curve for S_1, t, and $z = 0$. Figure III-B-2 shows such curves for $t = -30$, -26, -22, -18, -14, and -10 sec, $z = 0$, and both S_1 and S_2. Note that the possible position curve for a sensor originates at that sensor, which is the point on the curve corresponding to $t_1 = t$, unless the available measured azimuth curve begins after time t.

At time t, the plane must be at the intersection of the S_1 and S_2 curves for given t and z, assuming that the plane is actually at height z. Thus, for each t we get a plane location. Connecting these locations with straight lines gives the computed plane path displayed in Fig. III-B-2 which is just about equal to the actual plane path, so the actual path is not displayed. The plane is actually flying a straight line at Mach 0.9 and height 0.1 km. The difference between the assumed height $z = 0$ and actual height 0.1 km results in negligible error.

The possible position curves for $t = -22$ and -18 have multiple intersections: the extra intersections are labeled G, denoting ghosts. A crude automatic algorithm has been used in all our examples to distinguish real position measurements from ghosts, and to trace the computed path.

2. Azimuth Errors

We now consider the effects of errors in azimuth measurement. Suppose each such measurement ϕ is replaced by a range of measurements $(\phi - e, \phi + e)$, where e is the maximum

possible error in ϕ. Then, each possible position curve is replaced by a region shaped like a highway. The boundaries of this region are just the possible position curve rotated by $+e$ and $-e$ degrees around the sensor. Figure III-B-3 shows these possible position regions for $t = -30$, -18, and -6 with $z = 0$ and $e = 5°$. Also shown are the computed path, plus the ghosts for $t = -18$.

For particular t and z, the intersections of the S_1 and S_2 possible position regions determine an intersection region where the plane will be found. This region generally contains all plane locations and ghosts found in the previous section for given t and z. Basically, ghosts are the result of nearly tangentially intersecting possible position curves, and are associated with an elongated intersection region containing the true position plus ghosts. Noise in the azimuth readings can cause ghosts anywhere in the intersection region.

The intersection angle of the S_1 and S_2 possible position curves indicates whether the intersection region will be elongated. For mathematical reasons, we consider this angle to have a range from 0 to 360°, with 180° being the usual angle for tangential intersection. Angles between $180° - 2e$ and $180° + 2e$ will generally result in elongated intersection regions, whereas angles near 90° or 270° will generally result in small rectangular intersection regions. The intersection angle can be computed as follows. From the point at which the plane is located, draw three velocity vectors (see Fig. III-B-4):

$\bar{v}$	Plane's apparent horizontal velocity.
$\bar{v}_1$	Points at S_1 and has magnitude (speed of sound)/$\cos \Theta_1$, where Θ_1 is the elevation angle of the plane at the given point (depends on z).
$\bar{v}_2$	Similar to $\bar{v}_1$, but for S_2 and Θ_2.

Then, the direction of the S_1 possible position curve going through the point is $\bar{w}_1 = \bar{v} - \bar{v}_1$, and of the S_2 curve is $\bar{w}_2 = \bar{v} - \bar{v}_2$.

As an aside, we indicate why the above procedure works. At time t, the plane is at the given position, emitting sound received by S_1 at time t_1 and angle ϕ_1. At time $t + dt$, the plane has moved by an incremental position $dt\ \bar{v}$, emitting sound received by S_1 at time $t_1 + dt_1$ and angle $\phi_1 + d\phi_1$. Let $\bar{w}_1$ be a vector directed along the possible position curve for S_1, such that moving an incremental position $dt\ \bar{w}_1$ from the original position will also correspond to the same change $(dt_1, d\phi_1)$ in the azimuth curve for S_1. Consider the local rectilinear coordinate system $\bar{i}_r, \bar{i}_\phi, \bar{i}_\Theta$ at the aircraft location associated with global spherical coordinates with origin S_1, where $\bar{i}_r$ is the unit vector directed from S_1 to the given position, $\bar{i}_\phi$ is the unit vector in the direction of increasing ϕ, and $\bar{i}_\Theta$ is the unit vector in the direction of increasing Θ. Then, if r_1 is the horizontal distance between S_1 and the plane location,

$$d\phi_1 = dt(\bar{v} \cdot \bar{i}_\phi)/r_1$$

$$d\phi_1 = dt(\bar{w}_1 \cdot \bar{i}_\phi)/r_1$$

$$dt_1 = dt + dt(\bar{v} \cdot \bar{i}_r/\text{speed of sound})$$

$$dt_1 = dt(\bar{w}_1 \cdot \bar{i}_r/\text{speed of sound}) \quad .$$

These last equations imply

$$\overline{w}_1 \cdot \overline{i}_\phi = \overline{v} \cdot \overline{i}_\phi$$

$$\overline{w}_1 \cdot \overline{i}_r = \text{speed of sound} + \overline{v} \cdot \overline{i}_r \quad .$$

The equations just given imply $\overline{w}_1 = \overline{v} - \overline{v}_1$, where $\overline{v}_1$ is chosen so that

$$\text{speed of sound} = -\overline{v}_1 \cdot \overline{i}_r$$

$$0 = \overline{v}_1 \cdot \overline{i}_\phi \quad .$$

While $\overline{v}$ is the apparent horizontal velocity for the computed path, and not the plane's actual horizontal velocity, we will ignore the distinction here because the difference between these velocities will be small as long as the error in position due to mis-estimated height z is small. (If the position were accurate, both these velocities would be the same, because they give the same rates of azimuth change for S_1 and S_2.) Note, however, that an actual vertical component to the plane velocity is equivalent to a radial horizontal component, because it projects on $\overline{i}_r$, but that this equivalent horizontal component is different for each sensor, and cannot be expressed by changing the apparent horizontal velocity of the plane. So, our calculations are not exact unless the plane actually has zero vertical velocity, or unless the assumed height z = 0.

For given z and $\overline{v}$, curves of constant intersection angle can be plotted in the horizontal plane. These constant intersection angle curves have sensors as end points, and are shown in Fig. III-B-5 for z = 0 and the actual plane velocity $\overline{v}$. We call the region in which the intersection angle (ia) lies between 180° − 2e and 180° + 2e the region of linear ambiguity, because in that region plane position can only be localized in one dimension.

Comparison of Figs. III-B-3 and III-B-5 suggests that the intersection angle is not a very precise measure of how well a plane is localized. The region of linear ambiguity is nonetheless a useful descriptive concept.

Figure III-B-6 shows the computed paths of the four corners of the intersection regions for times including those of Fig. III-B-2. The intersection regions tend to lie between the outermost of these four paths. One clearly sees the changes in length of the intersection regions as the intersection angle changes. Near the region of linear ambiguity, the corners of the intersection regions exchange positions relative to each other, with their computed paths crossing over each other.

3. Errors in Assumed Height

Figure III-B-7 displays the computed plane paths for three different assumed heights: z = 0, 1, and 2 km. Not much change is observed as z changes, except in the region of linear ambiguity.

Figure III-B-8 is just Fig. III-B-2, but with assumed height z = 2 km instead of z = 0. Note that not only have the ghosts disappeared, but there is also no intersection at all of the possible position curves for t = −18 sec. Errors in azimuth can also eliminate intersections.

Possible position curves for t = 0 and z = 0, 1, and 2 are displayed in Fig. III-B-9. Changes in z only cause changes in the radial distance to the sensor, and therefore change the possible position curve significantly only when that curve is perpendicular to the radial direction from the sensor. Maximum perpendicularity is achieved by fast (nearly Mach 1.0) planes flying

almost toward the sensor. But if such a plane is between the two sensors, it will have a nearly radial possible position curve for the other sensor, and, consequently, the possible position curve for the other sensor will not change much with changing z. So, changing z in Fig. III-B-9 moves the intersection point along one of the two intersecting possible position curves.

Changing z induces a radial translation in a possible position curve very similar to the radial translation induced by changing t. Thus, changing z in Fig. III-B-9 moves the intersection point along the actual path. As a result, mis-estimating z does not mis-estimate the plane path, but only the times at which the plane is at various points on that path.

For planes flying between the sensors, changing z generally results in a position error parallel to the plane path.

4. Conclusions

Time series azimuth measurements from just two sensors, plus an estimate of plane height, can be used to locate a plane within a box, the intersection region of two possible position regions. For approximately half of a typical plane path, this intersection region is a nicely behaved rectangular box, but elsewhere the region is elongated and may become U-shaped. The major exception to this rule occurs when the plane flies along the straight line through the sensors, passing very near both sensors.

For two sensors 10 km apart, and planes flying no higher than 1 km, the effect of mis-estimating the plane height is usually minimal.

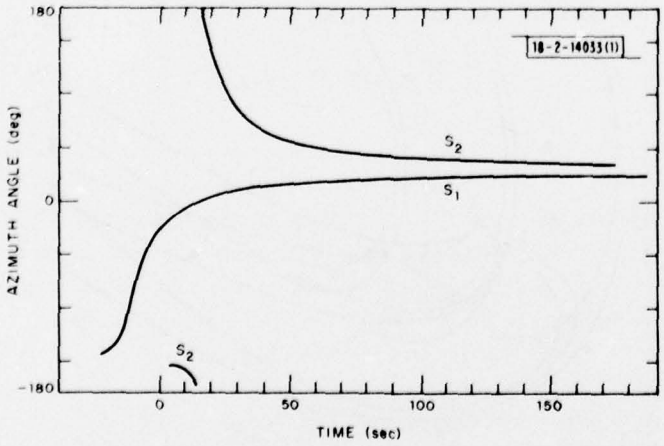

Fig. III-B-1. Azimuth angles vs time measured by sensors S_1 and S_2 for some aircraft to be located.

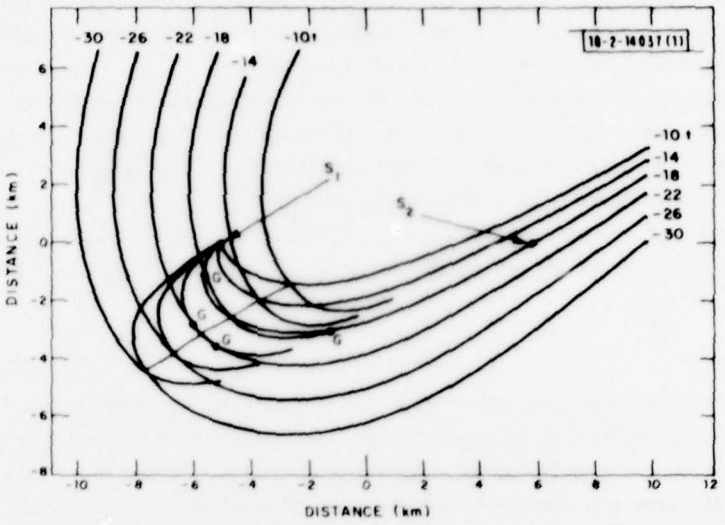

Fig. III-B-2. Possible position curves for t from −30 to −10 sec. There is one curve for each sensor, S_1 and S_2, and intersections of these two curves are either points on computed plane path (nearly straight line) or ghosts (marked G). Assumed plane height is z = 0, actual height is 0.1 km, plane velocity is Mach 0.9.

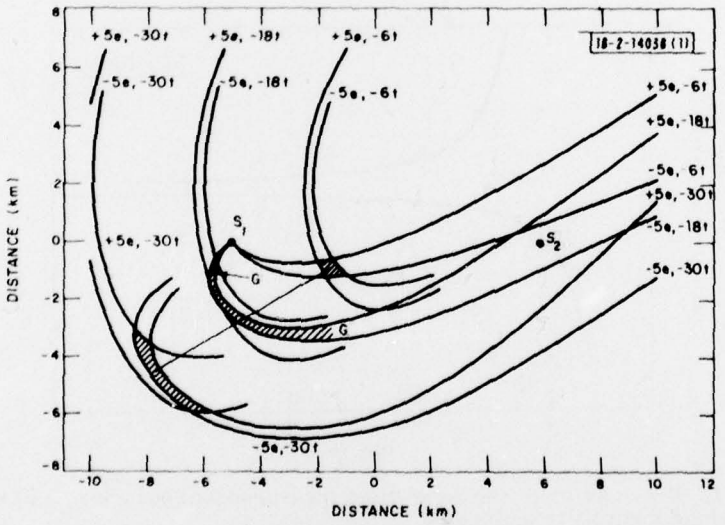

Fig. III-B-3. Possible position regions and intersection regions for times −30, −18, and −6 sec. Computed plane path (straight line) and ghosts (marked G) for these times are also plotted. Possible position regions are bounded by possible position curves with assumed errors e of +5° and −5°. z = 0 as for Fig. III-B-2.

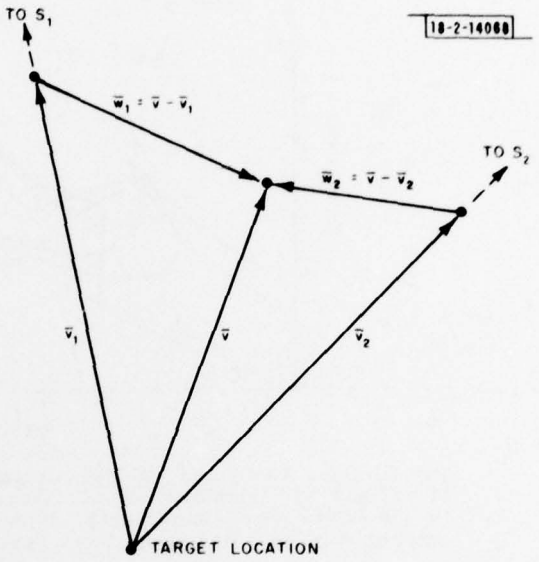

Fig. III-B-4. $\bar{v}$ is plane's apparent horizontal velocity. $\bar{v}_1$ is directed toward S_1, $\bar{v}_2$ toward S_2. If assumed height z = 0, magnitude of $\bar{v}_1$ and $\bar{v}_2$ is speed of sound. $\bar{w}_1$ is directed along S_1 possible position curve, and $\bar{w}_2$ along S_2 possible position curve.

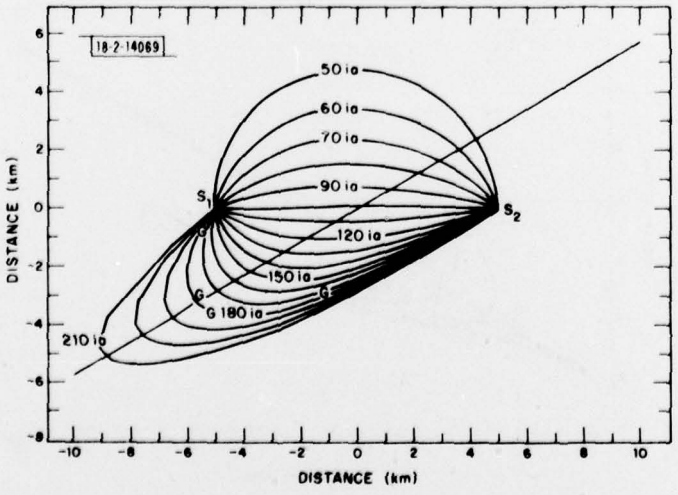

Fig. III-B-5. Curves of constant intersection angle, for angles from 50° to 210° in 10° increments. Plane's actual velocity is used with assumed height z = 0. Computed plane path and ghosts are displayed. Region of linear ambiguity lies between 170° and 190° curves.

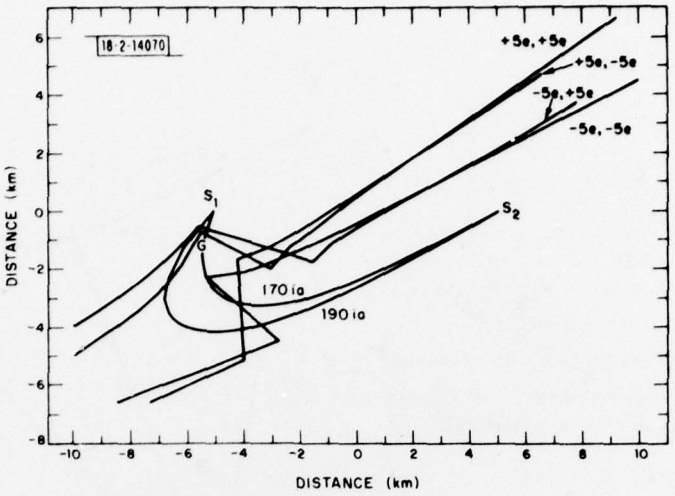

Fig. III-B-6. Computed paths of corners of intersection regions for errors e of +5° and −5° in azimuth angle, assumed height z = 0, and times from −50 to +50 sec in 4-sec increments. Intersection regions generally lie between outermost paths. Region of linear ambiguity is also shown.

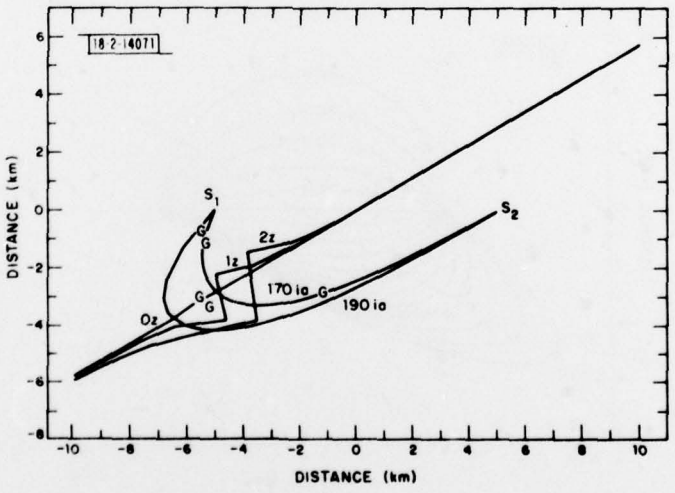

Fig. III-B-7. Computed plane paths for assumed heights z = 0, 1, and 2. Plane location is determined at times from −50 to +50 sec in 4-sec increments. Region of linear ambiguity is also displayed.

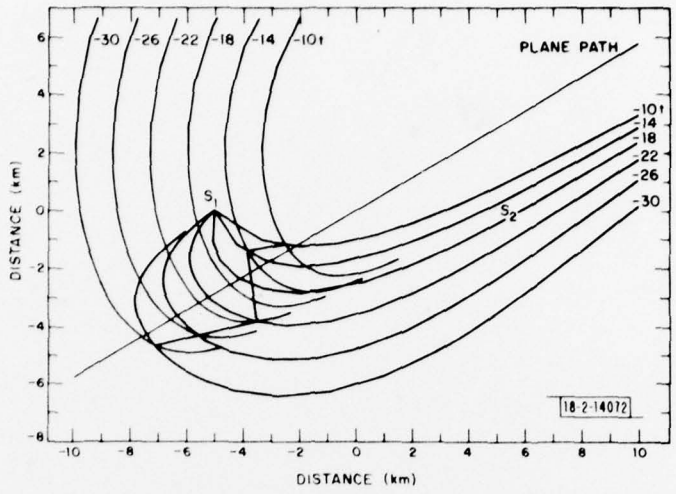

Fig. III-B-8. Possible position curves for assumed height z = 2 km and times from −30 to −10 sec. Actual plane height is 0.1 km. Actual and computed plane paths are displayed. At t = −18 sec, possible position curves do NOT intersect at all.

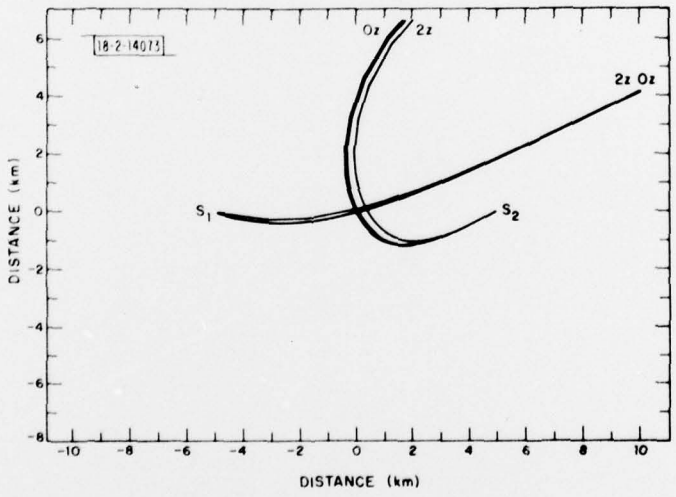

Fig. III-B-9. Possible position curves for time t = 0 and assumed heights z = 0, 1, and 2 km.

IV. GENERAL SYSTEM ANALYSIS

One fundamental issue for a surveillance system is the optimization of nodal geometry. Should a DSN consist of a few very powerful sensors or a large number of less-capable sensors? During this reporting period, our work in the area of general system analysis has concentrated upon a limited aspect of this question. The issue is a complex one involving communications, system cost, performance, reliability, survivability, and other factors. An initial analysis has been completed which has focused upon total system cost, sensor cost, the overlap in sensor coverage, sensor performance, and signal-path-loss factors. The analysis makes explicit some basic system trade-offs. This study was to identify and clarify issues and not to generate definitive answers to specific design questions. The analysis concentrated upon the surveillance of two-dimensional regions.

Suppose an area $A = 100 \times 100\ km^2$ is to be covered using sensors which each have a target acquisition range of R km. Figure IV-1 shows the number of sensor sites required and the total system cost for different costs per sensor. In constructing the figure, we assumed that sensors can cover a disk of area and that sensors are placed on a square grid of points, and that grid size is adjusted to the largest value which leaves no point uncovered by at least one sensor. Figure IV-2 shows this arrangement. Obviously, other packings and rules of coverage could be used, and we have selected a reasonable one for specific discussion. This packing gives an area coverage redundancy factor $\rho = \pi/2$, which was used in constructing the figure. Communication costs are assumed included in the sensor site costs. Figure IV-1 involves all basic system attributes of interest in our preliminary analysis of sensor performance and density issues except for propagation path loss. Some discussion of this figure will serve to motivate and introduce the subsequent analysis.

For A and ρ as specified above, we note that a system using sensor sites with a range of 23 km and costing $500,000 each would result in a total system cost of 5 million dollars. Suppose there is an option to use $50,000 sensor sites. If the range of the less-expensive sensor is greater than 7 km, the total system cost will be less for the large number of less-expensive sites. This issue, trade-off between sensor cost and range, is central to the analysis which follows. The analysis is to clarify issues and increase understanding. It should not be interpreted as a definitive solution to the question of optimum sensor distribution.

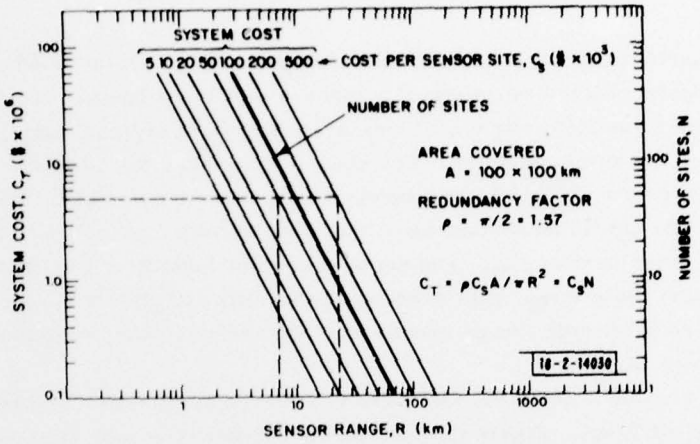

Fig. IV-1. Total system cost for a 100- × 100-km area as a function of maximum sensor range. Sensor packing is as shown in Fig. IV-2.

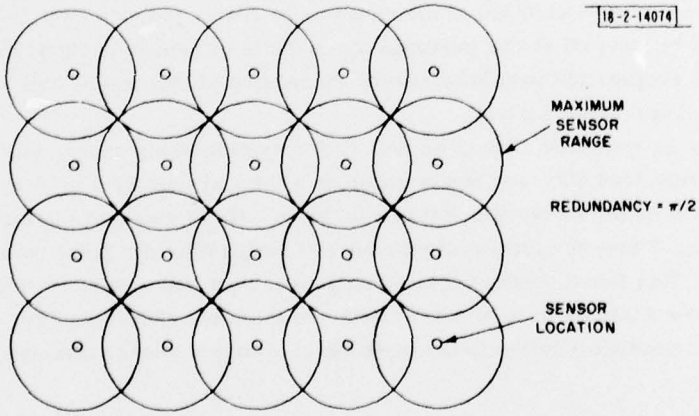

Fig. IV-2. A sensor packing strategy giving no holes in coverage.

A. COST MODEL IN TERMS OF SNR GAINS

For a passive sensor system, the basic signal-to-noise ratio (SNR) at a sensor site depends on the range to the target and the target signal strength. The sensor output SNR can be increased by signal processing, reducing system noise, the use of multiple sensors combined as an array, or some other method of obtaining directivity. This is true for systems involving passive sonar, atmospheric acoustics, IR sensors, seismic sensors, etc. For an active system, the basic SNR at a site depends on range, the power radiated in the direction of the target, and the target cross section which defines the effectiveness of the target as a re-radiator of power in the direction of the receiver. The SNR can be increased by signal processing, increasing the power radiated toward the target, increasing the directivity of antennas, or reducing receiver noise levels. Our basic sensor cost model for active and passive systems is that sensor cost is a monotonic increasing function of the SNR gain of the sensor.

Consider a minimal sensor of some type with an effective operational range of R_0 for targets of interest. The value of R_0 will depend upon the target type, but we assume that this is fixed for our analysis. We also assume that, all other factors being fixed, sensor cost is a function of sensor output SNR. For this purpose, SNR is defined as a power (squared amplitudes or mean squared values) ratio. Let G be the SNR gain of an enhanced sensor relative to the minimal sensor. The model for the cost of a sensor is

$$C = C_0 + C_1 G^c$$

where C_1 is the incremental cost per unit of SNR gain, and c is a positive number. Note that the reference sensor cost is $C_0 + C_1$, not just C_0. In what follows, we will deal with the cases $c = 1$ and $c = 1/2$.

A few examples will indicate that this model is a reasonable one for a number of situations of interest. Consider a passive system using microphones, seismometers, or hydrophones. The most common way to improve the capability of an individual site is to install multiple sensors and to operate the site as an array. To first order, it is reasonable to assume that the site cost will be a linear function of the number of instruments used in the array. But if the signal is coherent across the array and there are no special noise conditions, the array will effectively reduce the background noise power level by a factor of N – where N is the number of sensors in the array. A reduction of noise power by a factor of N is the same as increasing the output SNR by a factor of $G = 1/N$. Thus, our cost model should be applicable to a wide range of passive systems with the exponent c set equal to unity. For such passive systems, the natural reference sensor site is one containing a single sensor (microphone, etc.).

The situation is a little more complicated for active systems. First, we consider situations which seem reasonable for $c = 1$. The SNR of an active radar or sonar can be increased by increasing the peak radiated power or increasing the pulse lengths or integration times. The SNR is linearly proportional to peak radiated power and to integration time. Increasing integration time, particularly in a digital system, could result in a linear increase in processing costs. This would tend to justify our cost model with c = unity. It is also reasonable to assume that sensor cost will increase linearly with peak power. A simple argument to support this is to note that two equal-power sources can be combined to give an effective single source of twice the power and twice the cost of either of the small sources. Thus, an increase in peak power level can also be associated with a cost model having c equal to unity. Finally, for the $c = 1$

case, consider that a cylindrical array of horns is used for either transmitting or receiving, but not both. To first order, the antenna power gain will be directly proportional to the number of horns needed to cover all azimuths, and so will the cost of such a configuration. If horns are used for both transmission and reception, the cost still remains a linear function of the number of horns but the SNR gain goes as the square of that number. This is the important case for which $c = 1/2$.

Our model of sensor site cost assumes that communication costs are included in C_0. This is reasonable since we assume communication by a distributed packet switched communication system of the Packet Radio Net (PRN) class and that the PRN single-hop range is at least as large as the distances between adjacent sensor sites. For such a system, C_0 is bounded from below by the cost of a PRN site. Systems using hardwire communication or needing extra repeaters would require more-complicated modeling, and would generally increase the pressures to select more-powerful sensor sites.

With the above model for single sensor site cost, the model for total system cost is very simple. Specifically, as used in our introductory figure,

$$C_T = \rho CA/\pi R^2$$

where A is the area to be covered, πR^2 is the area of the disk covered by a single site with effective range R, and ρ is a redundancy factor.

B. CONVERSION OF COSTS TO A RANGE FUNCTION

If a power gain of $G > 1$ is obtained for a sensor site, this will increase the effective range from R_0 to some $R > R_0$. The amount of increase in range depends on the path loss experienced by the signals. A convenient model for path loss is that the power loss as a function of range is of the form

$$L(R) = R^{\lambda}$$

where λ is a positive real number. For this model, the extended range of a sensor as a result of a gain G in SNR is the solution of

$$G = (R/R_0)^{\lambda} \quad .$$

Using this, the cost of a sensor site becomes

$$C = C_0 + C_1(R/R_0)^n$$

where $n = \lambda c$ depends upon both the path loss model exponent λ and the SNR gain cost exponent c. With this the total system cost, in terms of the range of a single sensor, becomes

$$C_T(R) = (\rho A/\pi)\,[C_0 R^{-2} + C_1 R^{n-2} R_0^{-n}] \quad .$$

In the next section, we discuss the mathematically optimum selection of a sensor range. To facilitate that discussion, we include here a brief review of the physical significance of our path loss model for different exponents. Imagine a target radiating energy from a point in a homogeneous three-dimensional space. Such a situation involves spherical spreading. Signal power density is an inverse squared function of the distance from the radiator. This follows directly from the fact that the surface area of a sphere is $4\pi R^2$. Thus, our path loss model with $\lambda = 2$ is appropriate for a passive system with the signal subject to spherical spreading. Other passive sensor situations lead to less path loss. For example, acoustic signals in the atmosphere or ocean can be trapped within a two-dimensional waveguide so that the spreading of signals is in two dimensions rather than three. This is the case of cylindrical spreading, and corresponds to a path loss model with $\lambda = 1$. Finally, one can have more path loss than spherical spreading so that $\lambda > 2$. This can happen, for example, if the medium itself is very lossy, if variations in the medium result in strong shadow zones, or if there are other physical obstructions to the propagation. A nominal value of λ for scattered or diffracted signals, which are of some interest to us, is $\lambda = 4$.

The situation with active systems is similar, but we must use path loss models with twice the exponent value used for passive systems. For example, consider a radar system. The physical propagation involved is spherical, exclusive of terrain, foliage loss, etc. However, the spherical spreading occurs for the signal radiated from the transmitter and it also holds for the signal reradiated from the target. Thus, radar involves squared spherical spreading and corresponds to the path loss model $\lambda = 4$. In the case that the radar is line-of-sight (LOS) limited beyond R_0, an appropriate value for λ would be ∞. The value for diffracted radar would be $\lambda = 8$.

C. OPTIMUM STRATEGY AND DISCUSSION

Given R_0, C_0, C_1, λ, and c, we want to determine if a particular option for enhancing a sensor should be used. Clearly, if $C_T(R)$ is less than $C_T(R_0)$ for some $R > R_0$, then the site should be upgraded. Now we note that if $n = \lambda c$ is less than or equal to 2, then $C_T(R)$ is a monotonic decreasing function of R. In this situation the site should definitely be enhanced. Of course, this strategy is valid only as long as the model is valid. If n is greater than 2, then the value of R which minimizes the total system cost is obtained by setting the derivative of the cost to zero. This gives

$$R^* = R_0 \left[2C_0/C_1(n-2)\right]^{1/n} .$$

Depending upon the value of $2C_0/C_1(n-2)$, the strategy may be to enhance the site or reduce its capabilities. Large values of n will tend to push toward small sites, while small values of n will have the opposite effect. In terms of propagation loss, a similar trend is seen. That is, large propagation loss mitigates toward many small sensor sites, and small propagation loss favors a few powerful sites. Note that the redundancy factor ρ does not enter into the optimum choice of R, although it clearly affects system costs and performance.

Table IV-1 gives a more-physical interpretation of the implications of minimizing our expression for system cost for a number of different circumstances. In the table, the use of directivity for both transmission and reception is the equivalent of using an SNR cost model exponent $c = 1/2$. All other SNR improvement strategies correspond to $c = 1$.

First note that the use of directional antennas for both transmission and reception, within the context of our model and analysis, is a very cost-effective thing to do. For this SNR improvement option, one continues to increase directionality as much as possible so long as cost is linear with directionality and transmission loss is no worse than spherical. For radar, the obvious factor which impacts both of these is the LOS limit. When this limit is reached, it can be interpreted as a sudden switch to a propagation loss model which is much worse than spherical. This will cause us to stop trying to increase range by directionality. Also, one way to improve the LOS situation is to use well-sited and elevated radars. This, in turn, may cause the radar cost to increase at a much greater rate than that which is in our model. In any case, for active systems which can have directional gain increased at linear cost, we see that the trend is toward larger sensors up until other secondary factors make further enhancement practical or desirable.

Now consider the situations in which the SNR improvement strategy results in a linear relationship between SNR gain and sensor cost. That is, consider all SNR improvement strategies except using directivity for both transmission and reception. This includes all passive systems and some of the active options. Also exclude the case of LOS limited propagation since it is clearly a special case insensitive to SNR improvement strategy.

For active sonar the boundary where we always choose to enhance the sensor moves from the spherical to cylindrical propagation loss regime. That is, if loss is greater than cylindrical, then a limit to sensor enhancement will be reached. We point this out since cylindrical propagation is an important mode for underwater sound which is often trapped in a channel.

For passive systems in general, the boundary situation is the case of spherical spreading. This is true for passive sonar systems and for atmospheric acoustic systems. For example, if sound is trapped in a channel resulting in cylindrical spreading, then individual sensor sites clearly should be enhanced.

TABLE IV-1

OPTIMAL SENSOR RANGES FOR VARIOUS SYSTEMS, SNR IMPROVEMENT STRATEGIES, AND PROPAGATION LOSS MODELS

System	SNR Improvement Strategy†	Propagation Loss Model	Cost Exponent, n	Optimal Sensor Range, R
RADAR	D	Spherical or less	2 or less	Increase R
RADAR	D	More than spherical	>2	$R = R_0 [2C_0/C_1(n-2)]^{1/n}$
RADAR	Any	LOS limited	∞	$R = R_0$
Active SONAR	D	Spherical or less	2 or less	Increase R
Active SONAR	D	More than spherical	>2	$R = R_0 [2C_0/C_1(n-2)]^{1/n}$
Active SONAR	A, B, C	Cylindrical or less	2 or less	Increase R
RADAR	A, B, C	Spherical	4	$R = R_0(C_0/C_1)^{1/4}$
Active SONAR	A, B, C	Spherical	4	$R = R_0(C_0/C_1)^{1/4}$
Passive	A, C	Spherical or less	2 or less	Increase R
Passive	A, C	More than spherical	>2	$R = R_0 [2C_0/C_1(n-2)]^{1/n}$
Passive	A, C	Scattered	4	$R = R_0(C_0/C_1)^{1/4}$
Passive	Any	LOS limited	∞	$R = R_0$

† SNR Improvement Strategy Codes:

A. Directivity on transmission or reception only. In the case of arrays, increase the number of array elements.

B. Increase transmitter power of active system.

C. Increase pulse lengths or integration time.

D. Directivity used on both transmission and reception.

Finally, Table IV-1 includes three situations with n = 4. The passive system case with scattering as the principal propagation is of particular interest to us since it may be a reasonable model for acoustic surveillance of low-flying aircraft once the geometric shadow zone is entered. In this case, we see that our model asserts that sensor performance should be enhanced as long as C_0 is greater than C_1. The optimum sensor is that for which they are equal. One interpretation of this is as follows. In the model, C_0 includes the irreducible cost of a sensor site. For example, it includes the cost of the required communication system. The sensor itself may add to C_0, but it is clear that an optimum sensor site should cost at least twice as much as that irreducible cost.

REFERENCES

1. Semiannual Technical Summary on Distributed Sensor Networks, Lincoln Laboratory, M.I.T. (30 September 1977), DDC AD-A050160.
2. W. L. Wolf, Handbook of Military Infrared Technology (U.S. Government Printing Office, Washington, DC, 1965).
3. P. Borgart, Intern. Defense Rev. 4, 667-671 (1977).
4. J. A. Jamieson, R. H. McFee, G. N. Plass, R. H. Brube, and R. G. Richands, Infrared Physics and Engineering (McGraw-Hill, New York, 1963).
5. A. Jelalian, "Laser Radar Theory and Technology," in Radar Technology, E. Brookner, Ed. (ARTECH House, Dedham, MA, 1977), pp. 340-361.
6. B. Rossi, Optics (Addison-Wesley, Reading, MA, 1959).

UNCLASSIFIED

SECURITY CLASSIFICATION OF THIS PAGE *(When Data Entered)*

REPORT DOCUMENTATION PAGE		READ INSTRUCTIONS BEFORE COMPLETING FORM
1. REPORT NUMBER ESD-TR-78-208	2. GOVT ACCESSION NO.	3. RECIPIENT'S CATALOG NUMBER
4. TITLE *(and Subtitle)* Distributed Sensor Networks		5. TYPE OF REPORT & PERIOD COVERED Semiannual Technical Summary 1 October 1977 – 31 March 1978
		6. PERFORMING ORG. REPORT NUMBER
7. AUTHOR(s) Richard T. Lacoss		8. CONTRACT OR GRANT NUMBER(s) F19628-78-C-0002
9. PERFORMING ORGANIZATION NAME AND ADDRESS Lincoln Laboratory, M.I.T. P.O. Box 73 Lexington, MA 02173		10. PROGRAM ELEMENT, PROJECT, TASK AREA & WORK UNIT NUMBERS ARPA Order 3345 Project No. 7D30
11. CONTROLLING OFFICE NAME AND ADDRESS Defense Advanced Research Projects Agency 1400 Wilson Boulevard Arlington, VA 22209		12. REPORT DATE 31 March 1978
		13. NUMBER OF PAGES 64
14. MONITORING AGENCY NAME & ADDRESS *(if different from Controlling Office)* Electronic Systems Division Hanscom AFB Bedford, MA 01731		15. SECURITY CLASS. *(of this report)* Unclassified
		15a. DECLASSIFICATION DOWNGRADING SCHEDULE

16. DISTRIBUTION STATEMENT *(of this Report)*

Approved for public release; distribution unlimited.

17. DISTRIBUTION STATEMENT *(of the abstract entered in Block 20, if different from Report)*

18. SUPPLEMENTARY NOTES

None

19. KEY WORDS *(Continue on reverse side if necessary and identify by block number)*

computer network theory	acoustic, seismic, radar sensors
networking	low-flying aircraft
multisite detection	atmospheric propagation characteristics
target surveillance and tracking	packet radio

20. ABSTRACT *(Continue on reverse side if necessary and identify by block number)*

Progress on the Distributed Sensor Networks program is reported. Topics covered in the sensor area are the performance of acoustic sensors, sizing of acoustic front-end computation requirements, feasibility of adapting packet radios to perform as radar sensors, and a preliminary investigation of IR options. In all cases, the targets considered were low-flying aircraft or cruise missiles. Progress is reported in the area of decision theoretic surveillance space search methods of multisite detection and on specific algorithms to locate targets using two acoustic sites. Results of a preliminary parametric sensor and system cost analysis are given.

DD FORM 1 JAN 73 1473 EDITION OF 1 NOV 65 IS OBSOLETE

UNCLASSIFIED

SECURITY CLASSIFICATION OF THIS PAGE *(When Data Entered)*